NTNU
Norwegian University of
Science and Technology

# Design of a 5-axis Manipulator for Use in Angle-Resolved Photoemission Spectroscopy

Eirik Kjeken

Master of Science in Physics and Mathematics
Submission date: June 2016
Supervisor: Justin Wells, IFY

Norwegian University of Science and Technology
Department of Physics

**Abstract**

The design of a 5-axis manipulator for use in Angle-Resolved Photoemission Spectroscopy (ARPES) is presented along with an outline of the specific challenges it was designed to adress. The theory and nomenclature of X-ray Photoemission Spectroscopy and ARPES is reviewed. The lab at the Norwegian University for Science and Technology and its Ultra-High Vacuum chamber to be upgraded is introduced. Further upgrades to the detector and the purchase of a new X-ray gun is discussed, along with the possibility of utilizing oxygen $K_\alpha$ radiation from oxidization of the magnesium anode in the X-ray gun currently in use. To optimize results from this method, the anode voltage for maximum radiation intensity from the O $K_\alpha$ was determined to be 8 kV. Time constraints prevented proper testing and implementation of the finished manipulator.

**Sammendrag**

Designplanene for en 5-akse manipulator laget for bruk i ARPES målinger blir presentert sammen med en oversikt over de spesifikke utfordringene manipulatoren skal møte. Teorien og nomenklaturen bak XPS og ARPES blir gjennomgått. Laben på NTNU og UHV kammeret som skal bli oppgradert blir introdusert, og ytterligere oppgraderinger til detektoren og innkjøp av en ny røntgenpistol blir diskutert. Mulighetene til å bruke $K_\alpha$ stråling fra oksygen som har formet seg på magnesiumanoden til den nåværende røntgenpistolen blir undersøkt, og anodespenningen som gir høyest intensitet fra O $K_\alpha$ linjen ble bestemt til 8 kV. Forsinkelser og tidsbegrensinger forhindret testing og implementasjon av manipulatoren.

# Preface

This thesis is the culmination of a five year integrated master's programme called Applied Physics and Mathematics with specialization in Applied Physics. The studies were undertaken at the Norwegian University for Science and Technology (NTNU) over a six-year period from 2010-2016. The thesis has been written over a period of approximately five months, as the tenth and final semester of studies is fully committed to writing a master's thesis. The area of research for the thesis is largely up to the students own choice, and the intended audience is that of the student peers. Following this, it is assumed that the reader has basic knowledge of solid state physics and concepts employed in this branch of physics such as reciprocal space, Brillouin zone and the Fermi energy.

The project reported on here was conducted at the Section of Condensed Matter Physics under the excellent supervision of Associate Professor Justin Wells. Further supervision and invaluable support was provided by postdoc Dr. Simon Cooil. Appreciation and acknowledgements are owed them both. Dr. Simon Cooil deserves some extra credit for giving me permission to borrow figures and illustrations from his Ph.d. thesis. Ph.d. candidates Federico Mazzola and Marina Jorge also deserves acknowledgements for their company and support.

Ruland donated two flex couplings used in the design of the manipulator, and their generosity is greatly appreciated.

A final thanks goes out to my fellow master students Mathieu Børkja, Kristoffer Hunvik, Maxime Leclaire, Frode Strand and Jakob Vinje. They have all provided good company and an outlet to vent the stress and worries associated with writing a master's thesis.

# Contents

# 1 Background and motivation

X-ray Photoemission Spectroscopy (XPS) is one of the standard measurement techniques for obtaining chemical information about a sample, usually a solid. Being developed throughout the 50s and 60s, XPS has been actively employed for the last four decades, continually evolving in pace with technological progress. More brilliant X-ray sources along with more powerful computers and analyzers have resulted in new and exciting techniques, probing samples for previously unavailable information. One of these techniques is Angle-Resolved Photo Emission Spectroscopy (ARPES). When doing ARPES, one measures both the momentum and energy of the photoelectrons emitted from the sample. Using this information, one can construct the band diagram of the sample under investigation. ARPES is an extraordinarily powerful technique, and lies at the centre of this thesis.

The Norwegian University of Science and Technology (NTNU) houses several labs capable of XPS, but currently none of these labs are equipped for efficiently doing ARPES. The subject matter of this thesis is the upgrade of one of these labs to allow for ARPES measurements, with special emphasis on the design of a new manipulator. The lab in question is an XPS lab situated in the basement of the Natural Sciences building (room BU2-101). The lab is mainly used by a research group lead by associate professor Justin Wells, doing most of its research in Condensed Matter Physics. The lab consists of an Ultra-High Vacuum (UHV) chamber equipped with analyzers and light sources, as well as a rudimentary STM along with all the necessary pumps required for maintaining vacuum inside the chamber.

When upgrading the chamber for ARPES, one of the necessary changes turned out to be a replacement of the manipulator. The manipulator is the part holding the sample, and is responsible for all its movements and rotations within the chamber. Designing the new manipulator has by far taken up most of the semester. Finding ways to meet all the demands necessary for UHV conditions and ARPES while still keeping the manipulators size and manufacturing costs to a minimum has been a formidable challenge. To best equip the reader for understanding the physics behind these challenges and the presented soultions, the thesis will be structured in the following way; the thesis will start off with a chapter detailing the physical processes underlying XPS and ARPES. The operational principles of the analyzer involved in the measurements will also be reviewed. The lab will then be presented in the state it was in at the start of the semester, and the specific challenges that needed addressing in order to efficiently do ARPES will be explained in detail. Lastly, solutions to these challenges will be presented in the form of finished designs of new parts and their implementation.

# 2 Theory

This section seeks to equip the reader with the necessary theoretical knowledge for appreciating the physics underlying XPS and ARPES. The chapter will start out with a brief overview on XPS along with an outline of how an X-ray gun produces X-rays. ARPES will then be presented with an emphasis on the basic physical processes involved in the technique. Finally, the operational principles of an hemispherical analyzer (the type of analyzer typically employed in ARPES measurements) will be explained. The goal of this chapter is not to make the reader a technical expert on ARPES but rather to provide a basis for understanding what the technique demands of the lab equipment, as well as an appreciation of the information gained through ARPES measurements. When the specific upgrades to the lab at NTNU are presented later, the hope is that the reader not only understands what needed to be changed, but also why these changes were necessary.

## 2.1 X-ray Photoemission Spectroscopy

XPS has its beginnings in the discovery of the photoelectric effect by Heinrich Hertz in 1887. He observed that metals would expel electrons, dubbed photoelectrons, if illuminated with light of sufficiently high frequencies. Einstein later explained the photoelectric effect by positing that the X-rays consists of "packets of energy". This would later earn him a Nobel prize, and is widely regarded as the spark that lit the quantum revolution [1]. It was quickly realized that the photoelectrons could give insights to the electronic properties of materials if they could be appropriately measured. The development of XPS followed, spearheaded by K. Siegbahn working out of Lund university in Sweden. The culmination of his work was successful XPS measurements in the late 1960s [2] [3], which would award him the Nobel prize in 1981.

### 2.1.1 Physical principle

XPS is in the simplest terms done by illuminating a sample with X-Rays, then measuring the kinetic energy of the photoelectrons emitted from the sample. If the energy of the impeding photon is known, conservation of energy can be invoked to indirectly measure the binding energies of the atoms in the sample. The binding energy is the amount of energy required to excite an electron "free" from a bound state in an atom, and has an atom-specific value. Measuring these binding energies then allows for classification of the elements present in the sample.

The conservation of energy can mathematically be expressed as

$$\hbar\omega = E_k + E_b + \phi_s \tag{1}$$

where $\hbar\omega$ is the energy of the impeding photon, $E_k$ the measured kinetic energy of the photoelectron, $E_b$ the binding energy and $\phi_s$ the sample work function [4]. The work function is the energy required to remove the photoelectron from the sample to vacuum, and is a material-specific quantity. In all XPS measurements the sample is connected to an analyzer with a known work function $\phi_a$ of its own. This is the measure of the energy given up by the photoelectron as it is absorbed by the detector. If both the sample and the analyzers are electrically grounded through the same connection, a potential difference of $\phi_a - \phi$ between the sample and the analyzer arises[5]. This difference must be compensated in the energy conservation, which then reads

$$\hbar\omega = E_k + E_b + \phi_s + (\phi_a - \phi_s). \tag{2}$$

Simplified and rearranged for the binding energy the final equation yields

$$E_b = \hbar\omega - E_k - \phi_a. \tag{3}$$

The data from XPS measurements are typically expressed as an energy spectrum as shown in Figure 1. A sample is illuminated by X-rays, and the amount of photoelectrons with a given kinetic energy are counted up. A spectrum is then constructed expressing number of counted electrons as a function of their kinetic energy.

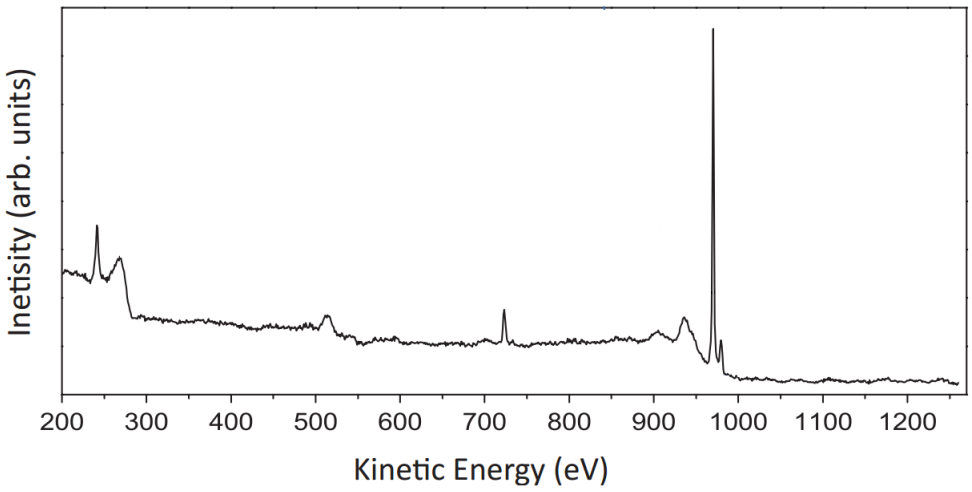


Figure 1: A typical XPS spectrum. This particular spectrum is collected from a diamond sample using Mg $K_\alpha$ X-rays. The peaks mark photoelectrons excited by the X-Rays with kinetic energies distinct for the atomic electron states. Figure adapted with permission from Ref. [5].

The vast majority of photoelectrons will lose energy on their way to the surface through interactions with atoms in the sample, resulting in very large intensities of electrons with a relatively low kinetic energy. This is known as the secondary electron tail[4]. Analyzers often ignore this part of the spectrum as the high intensity of electrons at these energies can

damage the instruments. Analyzing the secondary electron tail also requires additional calculations since the relevant information is "jumbled up", meaning there is no straightforward way to discern exactly what interactions the photoelectrons underwent on their way out to vacuum.

There are however a few electrons that will make it to the vacuum without interacting with the sample. The kinetic energy of these electrons will be described by equation (2), and will create distinct peaks in the spectrum. The binding energies corresponding to each peak can then be compared to table values of known atomic binding energies (typically the "Handbook of X-ray Spectrometry"[6]), and the sample can be chemically characterized.

### 2.1.2 X-ray guns and the XPS spectrum

To do XPS one needs a reliable source of X-rays. While the top facilities today create their X-rays with synchrotrons, the labs on the relevant scale to this thesis employ an X-ray gun. An understanding of the working principle of these X-ray guns is needed to appreciate some more subtle characteristics of an XPS spectrum.

All X-ray guns work by bombarding a metal target with accelerated electrons. An X-ray gun consists of an electron source and a target with an electrical potential difference between them, as shown in the simplified diagram in Figure 2. The electrons are usually generated through emission from a heated filament that also acts as a cathode. Conversely, the metal target acts as an anode. The potential difference accelerates the electrons emitted from the filament towards the metal anode, where they collide with the target. The accelerated electrons will interact with the bound electrons in the target material and excite the atom. The following relaxation will result in the emission of an X-ray with an energy characteristic of the electronic transition within the atom.

Electrons in all atoms have a large range of possible states, and the energy of the emitted photon is dependant on the specific transition within the atom. Different metal targets will have different transitions, and in turn different energies for the emitted radiation. The result is not a specific energy for the emitted X-rays, but rather a spectrum. In X-ray physics the standard notation is naming the orbitals after the principal quantum number n, starting with K for n=1 and following the alphabet with increasing n. The X-rays in the spectrum originating from a transition from an L orbital to a K orbital is then dubbed a $K_\alpha$ line, while a transition from the M orbital to the K-orbital would be a $K_\beta$ line. Further distinction between transitions from e.g. the $2p_{3/2}$ and the $2p_{1/2}$ (in atomic notation) orbital

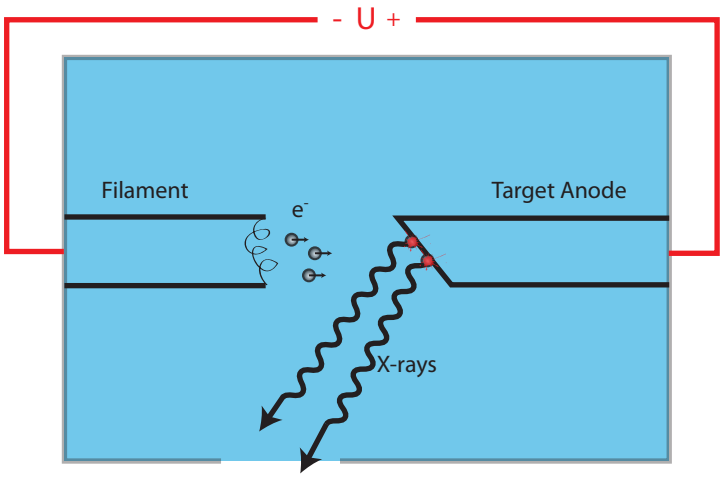


Figure 2: Simplified diagram of an X-ray gun. Electrons are emitted from a filament and accelerated towards the target anode by a voltage difference. The resulting collision produces X-Rays.

is noted by an additional numerical subscript, in this case $K_{\alpha 1}$ and $K_{\alpha 2}$ respectively. See Figure 3 for a graphical example.

The intensities of the different lines is proportional to the probability of each specific transition. Good elements for a target anode are then defined by having a dominant emission peak at the desired energy. Target materials often employed in XPS are aluminium and magnesium, where the $K_\alpha$ line dominates the spectrum with energies of 1487 eV and 1253 eV respectively [6].

In addition to the X-rays produced by transitions in the target material, all X-ray sources produce a continuous spectrum of radiation known as Bremsstrahlung. Bremsstrahlung literally translate from german as "breaking radiation" and is the result of electrons losing kinetic energy in the form of photons by interacting with matter, for example by inelastic collisions with other electrons present in the material. X-ray guns on the relevant scale are designed to reduce the background noise by covering the exit slit of the gun with an aluminum window. This window is designed to absorb some of the unwanted radiation, and has an absorption edge around the energy of the $K_\beta$ line of an Aluminum anode [7]. Some of the radiation will however still make it through and manifest itself as background radiation in the XPS spectrum.

One final note about X-ray guns is that the metals in the target anodes can get contaminated over time, typically by oxidization on the surface of the anode. The oxygen atoms

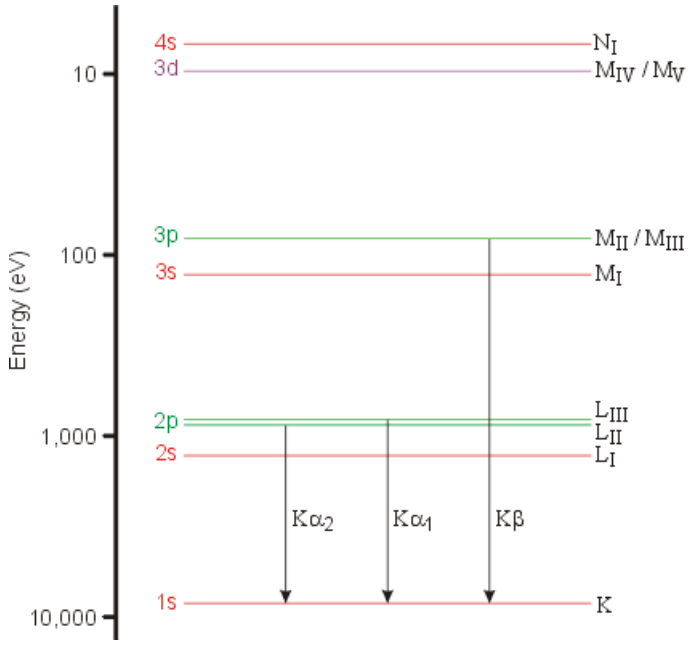


Figure 3: Diagram showing the relationships between atomic and X-ray notation. Binding energy is shown to the left, decreasing towards the loosely bounded valence states. Figure adapted from http://pd.chem.ucl.ac.uk/pdnn/inst1/xrays.htm

will then also be excited by the electron bombardment and emit X-rays of their own. These X-rays will excite photoelectrons that show up in the XPS spectrum as relatively low intensity peaks with an energy depending on the specific contamination material and transition, meaning that photoelectrons excited from the same orbital in the sample can manifest as two different peaks in the XPS spectrum.

## 2.2 Angle-resolved Photoemission Spectroscopy

Among the many different techniques that have their basis in photoemission, Angle-resolved Photoemission Spectroscopy (ARPES) is perhaps one of the most powerful to have emerged. The technique almost directly measures the momentum and kinetic energy of the electrons within a crystalline sample, which allows the band structure of the sample to be reconstructed. It has become an invaluable tool when investigating semiconductors, where the band structure plays a crucial role to the properties of the sample. With ARPES, one could for example directly observe the effect of doping a semiconductor sample. This section will give an overview of the physics underlying ARPES before a section detailing the functional principle of a hemispherical analyzer will close the theoretical part of the thesis.

### 2.2.1 Emission angles and momentum

As the name of the technique suggests, ARPES involves angles. By measuring the angle of emission $\theta$, the momentum $\hbar\mathbf{k}$ of the photoelectrons ($\mathbf{k}$ denotes the wave vector of the photoelectron), can be found by decomposing the momentum into components parallel and perpendicular to the sample surface

$$\begin{aligned} \hbar k_{\parallel} &= \sqrt{2mE_k}\cos\theta \\ \hbar k_{\perp} &= \sqrt{2mE_k}\sin\theta. \end{aligned} \tag{4}$$

Here, $m$ is the mass of the electron, $E_k$ its kinetic energy and $\theta$ the angle to the surface normal of the sample. It is important to note that this is the momentum of the photoelectron after it has reached vacuum, and is denoted by a lowercase vector $\mathbf{k}$. The energy states within the sample is a function of the corresponding uppercase wave vector $\mathbf{K}$. The crucial distinction is the boundary between the sample surface and vacuum, and the shape of the surface potential at this boundary. As the momentum within the sample $\mathbf{K}$ is the desired quantity to measure, conservation of momentum must be invoked to obtain relationships between the parallel and perpendicular components of $\mathbf{k}$ and $\mathbf{K}$.

Crystals are defined by their periodic arrangement of atoms, resulting in a periodic electronic wave function. If this wave function is considered at two points situated immediately inside or outside the crystal surface, translational symmetry is conserved across the boundary. As a consequence, the momentum parallel to the surface is conserved. Stated mathematically

$$k_{\parallel} = K_{\parallel}. \tag{5}$$

An intuitive way of understanding this is to consider the periodicity of the electromagnetic potential of the crystal as it decays into vacuum. The periodicity of the components of the field perpendicular to the surface will remain, even as the field strength falls off. The periodicity of the field components parallel to the surface will in contrast reach an abrupt stop once the surface is reached, as shown in Figure 4. As a consequence, the perpendicular momentum is generally not conserved;

$$k_{\perp} \neq K_{\perp}. \tag{6}$$

The usual way to counter this issue is to assume that the excited electron states $E(\mathbf{k})$ can be approximated by a free-electron model

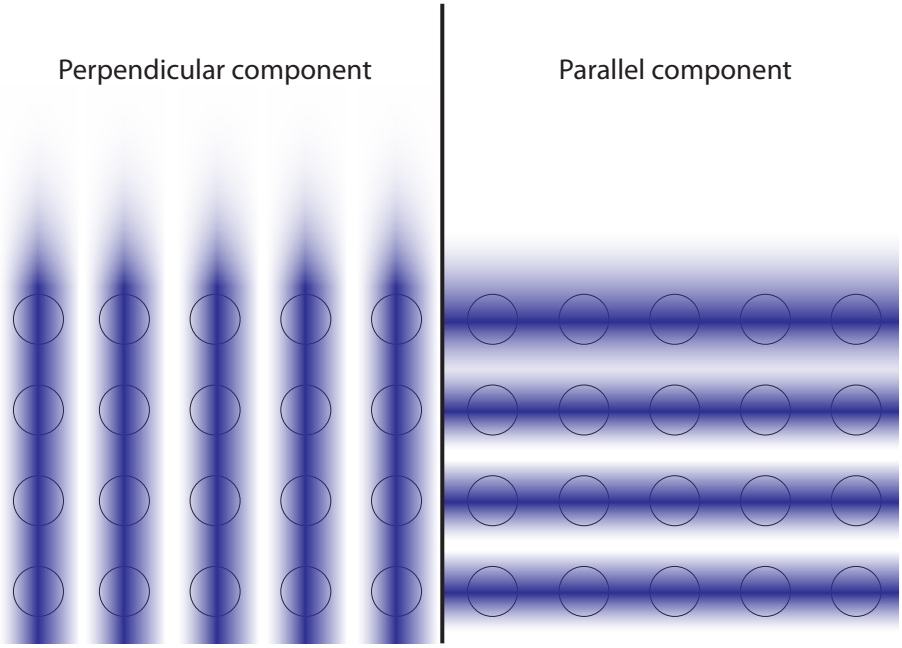


Figure 4: Figure illustrating the periodicity of the fields. The crystal is represented as an array of atoms. The perpendicular components of the fields maintain their periodicity across the boundary to vacuum, but the periodicity of the parallel component comes to an abrupt halt at the surface.

$$E(\mathbf{K}) = \frac{\hbar^2 \mathbf{K}^2}{2m} - |E_0|, \tag{7}$$

where $|E_0|$ is the energy of the electrons in their ground state in the atoms within the sample. It can then be shown that the perpendicular momentum inside the crystal can be expressed as

$$\hbar K_\perp = \sqrt{2m(E_k \cos\theta + V_0)}. \tag{8}$$

$V_0$ denotes the total energy required to excite the electron from it's band to the vacuum [5]. Equipped with the necessary relationships between the measured momentum $\mathbf{k}$ and the crystal momentum $\mathbf{K}$, it is possible to reconstruct a band dispersion diagram $E(\mathbf{K})$. Measurements over a certain range of $\phi$ gives a "slice" of the Brillouin zone in reciprocal space, and by rotating the sample around $\theta$ one can construct the electronic band structure. The sample can be further rotated azimuthally around $\phi$ to reorient the sample, making it possible to map the Brillouin zone to different high-symmetry points. This concept is illustrated in Figure 5. Figure 6 show a 3D cube of data constructed by multiple slices of ARPES measurements. Further information on ARPES can be found in e.g. the excellent paper "Probing the electronic structure of complex systems by ARPES" by Andrea Damascelli [8].

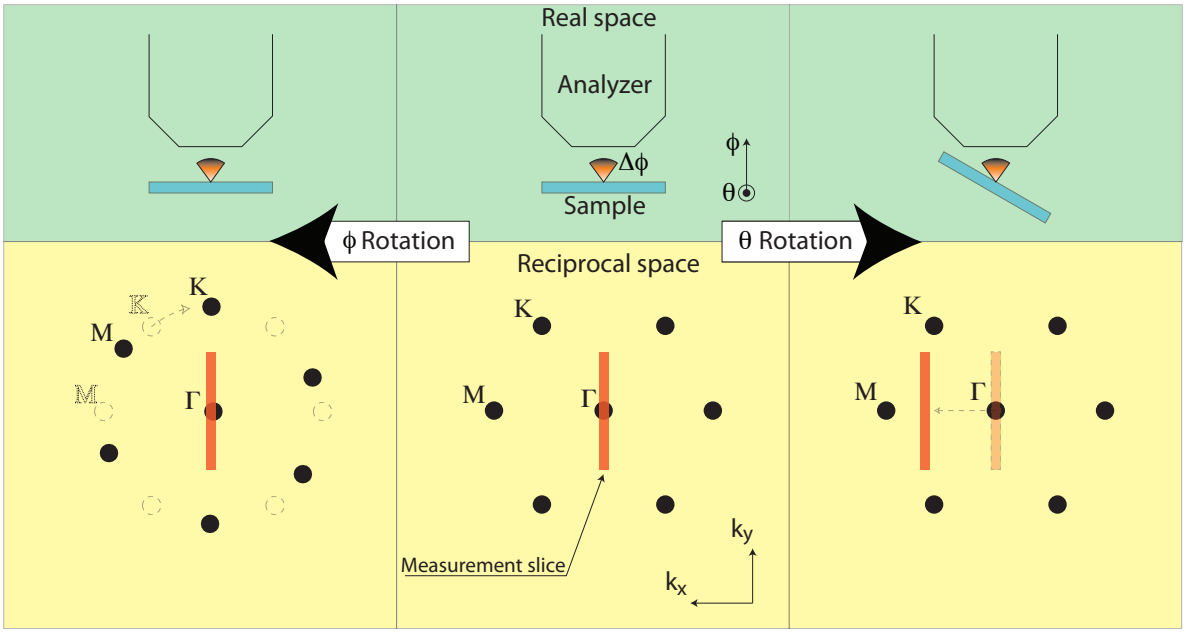


Figure 5: The effects of polar and azimuthal rotations on ARPES measurements. The analyzer measures photoelectrons emmitted over a certain range of angles $\Delta\phi$. The orientation of the sample in respect to the analyzer is shown in the top half, while the corresponding changes in reciprocal space are shown below. By polar rotations around $\theta$ a series of slices can be taken towards a high-symmetry point, allowing the dispersion relation to be constructed. Azimuthal rotations around $\phi$ reorients the sample, allowing the dispertion relation to be mapped over different regions of the Brillouin zone.

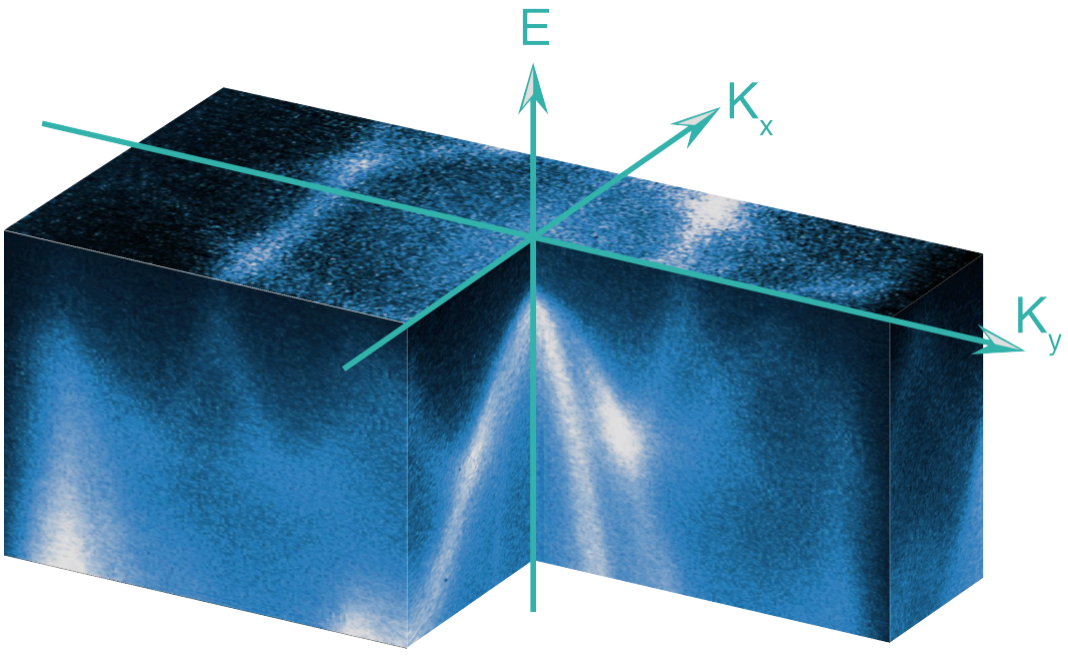


Figure 6: A cube of data constructed of slices in reciprocal space taken by ARPES. The cutaway reveals the 2D electronic band structures. Figure adapted with permission from Ref. [5].

### 2.2.2 The Hemispherical Analyzer

Although there are several different ways to detect and analyze photoelectrons in XPS and ARPES, all the measurements discussed here have been obtained using a hemispherical analyzer. The analyzer detects the energies of the photoelectrons by dispersion through electric fields. The electrons first pass through a stack of electrostatic lenses, that serve to focus and redirect the electrons along a path to the final detector. The stack of lenses connects to the namesake of the analyzer; two metal half-spherical shells with a voltage difference between them. The electrons with larger kinetic energies will have a slightly different path than electrons with lower kinetic energies, separating them as they travel through the hemisphere. The electrons finally crash into a detector situated on the opposite side of the hemisphere from the stack of lenses. A diagram of a hemispherical analyzer along with the orientation of rotation axes is shown in Figure 7.

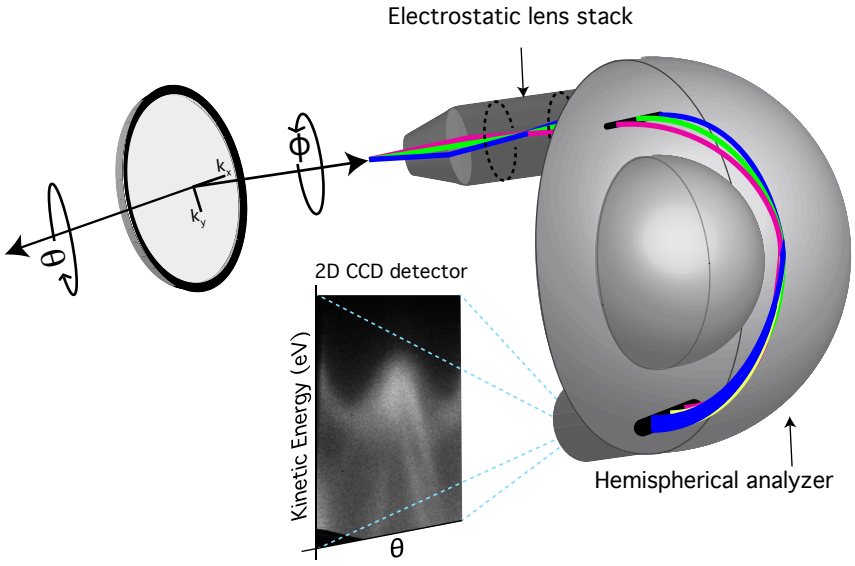


Figure 7: A model of a hemispherical analyzer showing the dispertion of the photoelectrons across the hemisphere. The different rotation axes are shown on the sample. The analyzer is equipped with a 2D detector, showing the energy resolved over a range of the emission angle $\theta$. Figure adapted with permission from Ref. [5].

The analyzer has a range of different parameters that can be changed and customized at the discretion of the experimentalist, including the size and shape of the entrance and exit slits to the hemisphere and the settings of the electric lenses. The energy resolution, angular resolution, count rate and whether or not real space or reciprocal space is examined all depend on these settings [9]. All this aside, the component of the analyzer that by far

has the most impact on measurements is the detector. The detector comes in two main variants; 1D and 2D.

A 1D detector is built up of several electron multipliers known as channeltrons. The channeltrons consists of electrodes that are design to emit secondary electrons if struck by a photoelectron. These secondary electrons will again hit the walls of the channeltron, causing a chain reaction resulting in a cascade of secondary electrons. This avalanche of electrons amplifies the signal strength of the initial photoelectron in their numbers. The secondary electrons finally hit an anode resulting in a measurable current spike [10]. In a 1D detector, several channeltrons are situated along the exit slit of the hemispherical analyzer. Each channeltron will detect photoelectrons of a certain kinetic energy. Although each channeltron will detect photoelectrons emitted across a small angle dispersion, this dispersion is not differentiated in the outgoing signal.

A 2D detector works along the same principle of a 1D detector. The basic component of a 2D detector is something called a Multi-Channel Plate (MCP). The MCP is a grid of small shafts that all acts as electromultipliers. In contrast with the 1D detector, the fact that the angular dispersion is now quantized along with the kinetic energy allows the measurement of energy as a function of emitted angle [11]. The MCP is typically placed above a phosphor screen that is illuminated when hit by the spray of electrons from the electromultiplier shafts. The light from this phosphor screen can then finally be detected by a CCD, which transmit an electronic signal that is measured.

# 3 The Laboratory

This section will present the XPS lab at NTNU along with the relevant components for this thesis. Figure 8 shows the Ultra-High Vacuum (UHV) chamber in its original state, before any of the upgrades discussed here. This chapter will examine the parts that are relevant for ARPES measurements (the X-Ray gun, the analyzer and the manipulator) and their specific limitations with ARPES in mind.

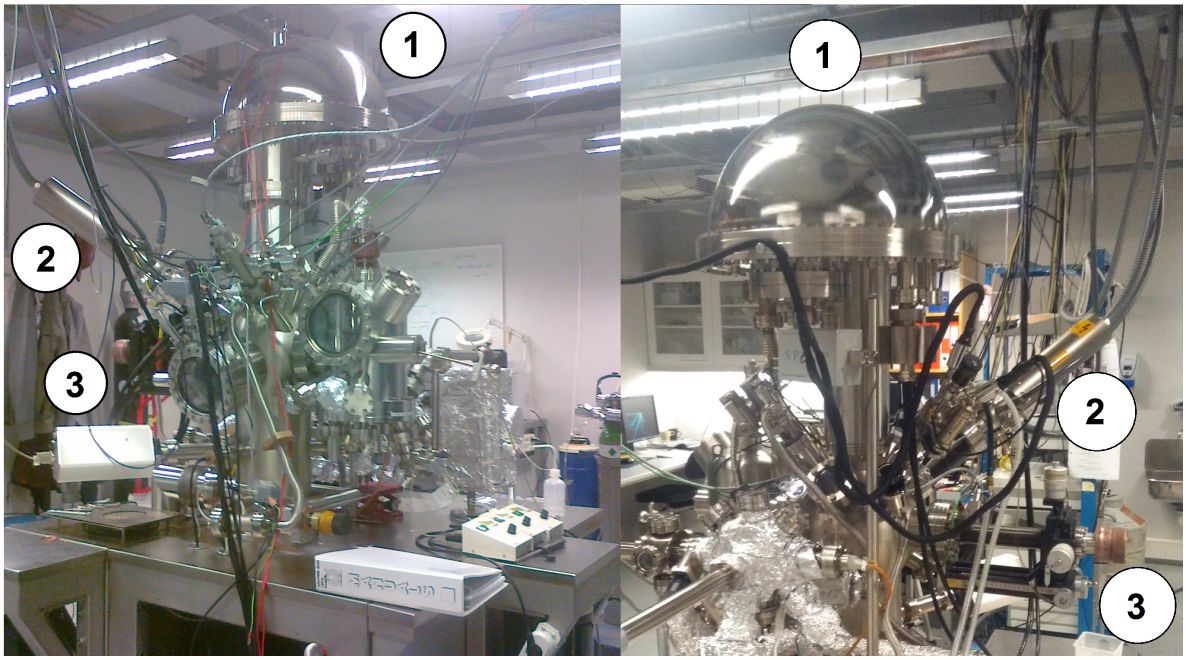


Figure 8: Two views of the UHV chamber in the lab at NTNU. The components discussed in the thesis are labeled; 1 marks the hemispherical analyzer, 2 the X-ray gun and 3 the manipulator.

## 3.1 The X-Ray Gun

The UHV chamber is equipped with an XR 50 X-Ray Source from SPECS. The gun has two targets anodes; Al with a $K_\alpha$ line of 1487 eV and Mg with a $K_\alpha$ line of 1253 eV [12]. There are three main issues with the X-Ray gun when doing ARPES. The issues will be addressed in turn; The polychromatic nature of the radiation, the spot size and the energy of the radiation.

### 3.1.1 Polychromatic radiation

Polychromatic radiation is simply radiation over multiple wavelengths (and hence energies). The effects of polychromatic radiation on emission spectra has already been discussed in the theory section, but its effects on ARPES measurements are still worth ex-

amining. The main consequence of the polychromatic nature of the radiation are the emergence of satellite peaks in the photoelectric emission spectrum. Furthermore, the X-Ray gun has been in use for several years, and the anode has been oxidized to the degree that significant emission peaks originating from an oxygen $K_\alpha$ line are present, and the extra photoelectrons emmitted from this radiation can contribute to wrongful data in ARPES measurements. With equation (3) in mind, a measured photoelectron originating from the O $K_\alpha$ line can be wrongfully attributed to the photon energy $\hbar\omega$ of the Mg $K_\alpha$ line of the target anode, resulting in a false measurement of a given binding energy.

### 3.1.2 Spot Size

This issue concerns the fact that the radiation emitted from the X-Ray gun is not focused. The sample is not illuminated on a specific spot, but rather evenly across an area. This means that photoelectrons emitted at large angles across the sample can make their way to the detector, as illustrated in Figure 9. The analyzer is ideally measuring photoelectrons emitted from a single point at the sample, and cannot distinguish between photoelectrons emitted from different points of the sample. The result is a broadening of the measured bands in the dispersion diagram, as electrons with the same energy are misattributed to emission angles that ideally should not have reached the analyzer.

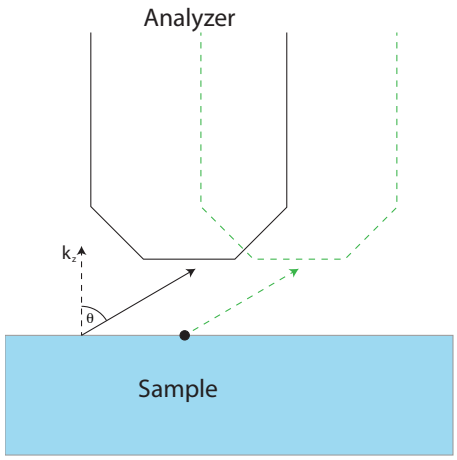


Figure 9: The effects of a large spot size. Ideally, the photoelectrons are emitted from a point directly under the entrance to the electrostatic lenses on the analyzer. The black arrow represents a photoelectron emitted a distance away from this point, with an angle $\theta$ that would cause it to miss the analyzer if it was emitted from the ideal location. The analyzer detects the photoelectron, but "sees" it as emitted from the ideal point, as indicated by the green outline.

### 3.1.3 X-Ray energies

The relatively high energy of the emission lines is another issue with respect to ARPES measurements. The probability of emitting an electron from its electronic state is given by a quantity known as the photoionization cross section. Although a full derivation of the cross section is outside the scope of this thesis, suffice it to say that the probability of exciting an electron decreases along with the difference between the binding energy of the electron and the energy of the impeding photon. When doing XPS and ARPES, this quantity is looked up in tables for the specific transition in question. A more thorough mathematical derivation of the photoionization cross section can be found in Ref. [13].

In ARPES one is usually interested in examining the states in the valence bands up to the Fermi level. These are the states that largely decide the electronic properties of a semiconductor, and are the states most sensitive to changes induced by e.g. doping. The binding energies of the states in the valence bands are usually on the order of hundreds of electron volts or less, meaning the highest probability of exciting electrons from these states is achieved with an X-ray energy of approximately a hundred electron volts. Given the characteristic energies of the anodes mentioned above at around a thousand electron volts the result is a relatively low probability of emission from the valence bands, resulting in low intensity measurements.

## 3.2 The Analyzer

The analyzer currently in use on the UHV-chamber is a PHOIBOS 150, originally designed for XPS and UPS by SPECS [14]. While the hemispherical analyzer itself is perfectly suitable for ARPES, the current detector presents a big obstacle for efficient measurements. The setup utilizes a 9-channel channeltron detector; a 1D detector described in the theory section. The detector measures photoelectrons with different kinetic energy over an angular range depending on lens mode ($\theta = \pm 1.5^\circ$ in Wide Angle Mode (WAM)). Doing ARPES with this setup requires many consecutive measurements, rotating the manipulator multiple times to account for the relatively low angle coverage. A full band diagram can then be constructed by a series of "strips", each strip representing a measurement of kinetic energy across the respective angle range (again, $\approx 3^\circ$ in WAM). Figure 10 illustrates this by comparing ARPES measurements taken of a $MoS_2$ sample collected in the NTNU lab using the current detector with measurements of the same sample taken at the University of St. Andrews in Scotland with a 2D detector.

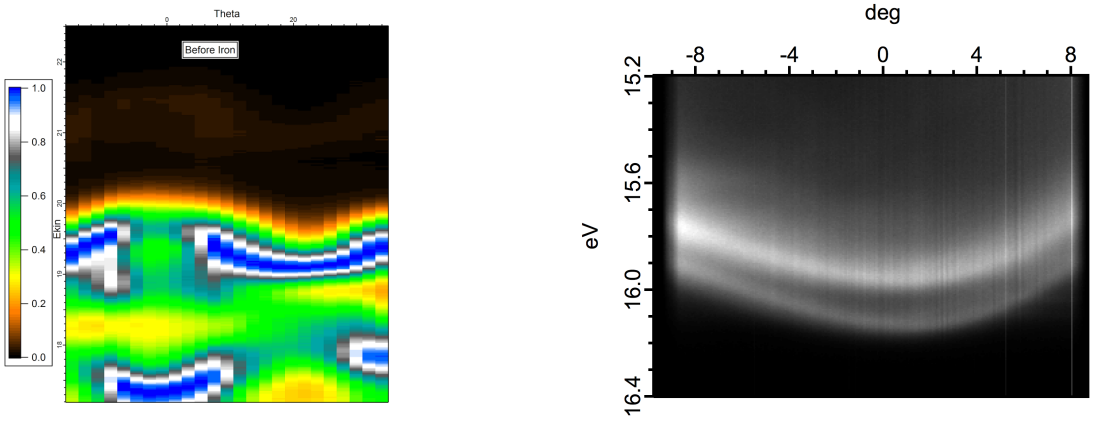


Figure 10: Comparison of two ARPES measurements of the same sample, with a 1D and 2D detector. The left plot shows ARPES taken at NTNU, while the right shows a portion of the same band structure taken at St. Andrews. The data from NTNU clearly shows the distinctive "strips" of the 1D channeltron detector.

## 3.3 The Manipulator

The manipulator that currently sits in the chamber is a design from Omicron NanoTechnology originally designed for Scanning Tunneling Microscopy. The manipulator has 4 degrees of freedom, meaning it can move the sample in x, y and z directions along with polar rotations around the $\theta$ axis.

By far the biggest limitation of the manipulator is its lack of azimuthal rotation around the $\phi$ axis. Azimuthal rotations dramatically increases the benefits from ARPES measurements, as the sample can be reoriented to image different high symmetry points in the Brillouin zone. The effects of polar and azimuthal rotations on ARPES measurements were illustrated in Figure 5. The lack of azimuthal rotations essentially means that measurements can only be done in the crystal orientation the sample happened to be in as it was mounted. Although ARPES is still possible, mapping to different high-symmetry points requires taking the sample out of the chamber and remounting it. This process is difficult and time consuming. As there are no guarantees for the orientation of the sample Brillouin zone in respect to the analyzer, extra calculations might also be needed to compensate for any such offset.

The design of a new manipulator to tackle this issue will be the focus of the next chapter.

# 4 Designing a new manipulator

Although the motivation for a new manipulator is the addition of azimuthal rotation of the sample, the new design has to tackle multiple additional challenges. The manipulator has to be suited for UHV conditions while still allowing both heating and cooling of the sample, all the while minimizing heat loss to the environment. The inside of the vacuum chamber is populated by sensitive equipment, and the manipulator has to allow for rotation and translation without collisions. As the list of challenges goes on, this chapter presents the final design of the new manipulator. Each feature of the manipulator will be explained along with the specific challenge it was designed to meet.

## 4.1 The features of the manipulator

Figure 11 shows the manipulator and its different parts. The manipulator will have four components that drive rotations and translations of the sample. These components supply the necessary force to move or rotate the sample given a manual input. Such components are called drives. Translations in x, y and z-directions along with polar rotation around the $\theta$ axis are achieved by three different drives purchased from Lewvac. The drives were chosen to provide the most stable and precise movement to the manipulator while still satisfying budget constraints. Table 1 shows the specific part codes for each drive. More information on the drives can be found in the downloadable catalouge at Lewacs websites [15]. In addition to the three drives, a multiport adaptor was designed and submitted to Lewac for manufacturing. The multiport adaptor allows all the necessary wires and cables to feed through into the sample stage. The multiport adaptor includes the drive for the azimuthal rotation.

Table 1: Part codes for components ordered from Lewac

| **Component** | **Part Code** |
|---|---|
| XY-drive | M-Z152-100/63CF |
| Z-drive | M-XY12-72-63CF |
| $\theta$-drive | M-RP-63CF |

### 4.1.1 Heating and Cooling

Along with translations and rotations, the manipulator is designed to allow for both cooling and heating of the sample. The ability to heat the sample is desirable for multiple reasons. When doping the sample surface it is often necessary to anneal the sample to allow the crystal structure to recrystallize. Annealing can also reduce the amount of dislocations and impurities in the crystal structure. Heating the sample can rid the crystal

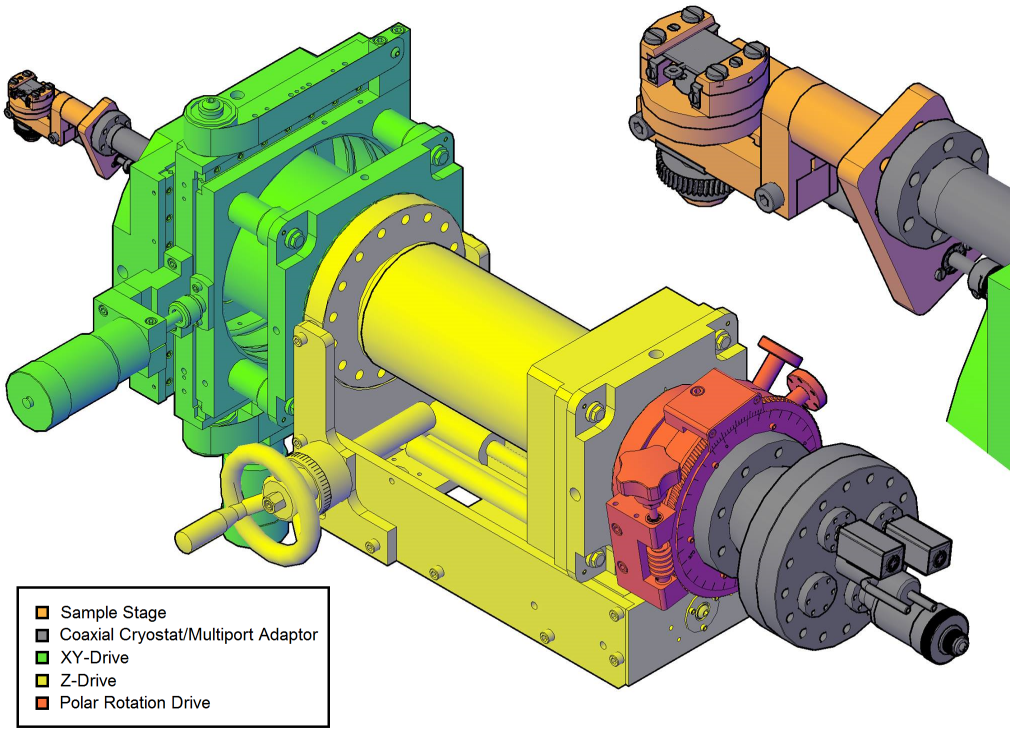


Figure 11: Computer model of the manipulator with the different parts labeled by color. A zoomed-in detail of the sample stage is seen in the top right corner. The manipulator will be connected to the vacuum chamber by a flange on the XY-drive, with the sample stage extended into the chamber by the Coaxial Cryostat.

of unwanted chemicals by evaporation. The manipulator is designed to heat the sample through e-beam heating, meaning that heating is supplied by accelerating electrons emitted from a light bulb filament on to the sample. The manipulator will additionally feature a thermocouple to measure the temperature of the sample.

Likewise there are many reasons to cool the sample. The most obvious reason is to reduce effects caused by thermal motion of the electrons in the sample. With higher temperatures the electrons have a larger distribution of average kinetic energy, and the result is a broadening in the energy bands caused by a larger uncertainty in the energy. Temperature also affects the total number of counts, as the photoelectrons are more likely to interact with the sample through for example inelastic collisions at higher temperatures. Finally, the temperature of the sample can affect the probability of a multitude of other effects, such as phonon-photoelectron coupling and structural phase transitions [16]. To control these effects and possibly study them, a mechanism to control the temperature of the sample is needed.

In the design, cooling of the sample is achieved by pumping liquid nitrogen through a

coaxial tube. This tube functions both as a cryostat and the main supporting arm holding the sample stage. A technical drawing of the cryostat and multiport adaptor can be found in Appendix II.

### 4.1.2 Floating and Grounding the Sample

The sample stages are designed to allow the user to put the sample either at electrical ground or at a potential. Putting the sample at a potential is known as floating the sample. As previously mentioned, the sample will be heated through e-beam heating. This requires the sample to be at an electric potential in order to accelerate the electrons towards it. Having the sample at a potential also allows measurement of the drain current of the sample, that is, the amount of current the sample will draw. This is handy when doing e.g. sputtering (cleaning the sample surface by bombarding it with positively ionized argon), as the sputtering positively ionizes the sample. A current of electrons will form to the sample to equalize the positive charge, and by measuring this current it is possible to determine when the sputter gun is aimed correctly at the sample.

Another effect of putting the sample at a potential is that you effectively displace the entire XPS spectrum with an amount equal to the applied potential. This allows the researcher to access regions of the spectrum previously unavailable. As previously mentioned, the XPS spectrum at the lower energies is dominated by the secondary electron tail. This tail has a sudden drop down to zero as the energy axis approaches the minimum energy required to excite a photoelectron out of the sample. This is initially not measurable, as a photoelectron at this edge will exit the sample with zero kinetic energy. By putting the sample at a potential, this drop is shifted into the measurable range.

Finally, when exciting photoelectrons from the sample it obviously has to be at ground potential, as an electric field would interact with the photoelectrons and disturb the measurements.

## 4.2 The Sample Stage

The sample stage is the part of the manipulator that holds the sample, and was entirely designed by Dr. Simon Cooil and the author. Plans for the design was submitted to the workshop at NTNU, and the all the parts were manufactured at the workshop. with the exception of a worm screw and the gear connecting to it. These two components were salvaged and recycled from an old manipulator. A rendered computer model of the sample stage design is shown in Figure 12, while Figure 13 shows the assembled sample stage after manufacturing. Figure 14 shows an exploded view of the manipulator. Detailed drawings

of each individual part, along with a list of screws used in assembly can be found in Appendix I.

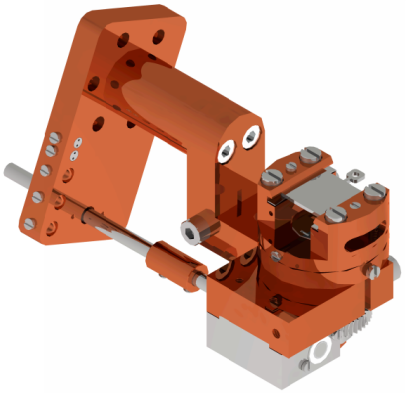

Figure 12: Rendered computer model of the assembled sample stage. The sample is mounted on the plate with the protruding handle.

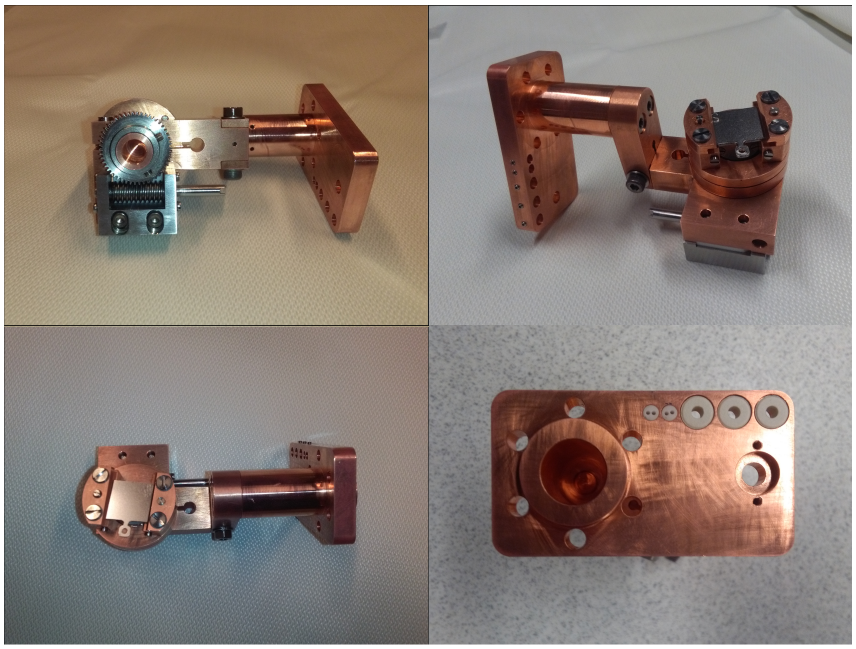

Figure 13: Different views of the assembled sample stage with sample plate. Note the worm screw mechanism driving the Azimuth rotations, and the wire feedthroughs with ceramic insulation.

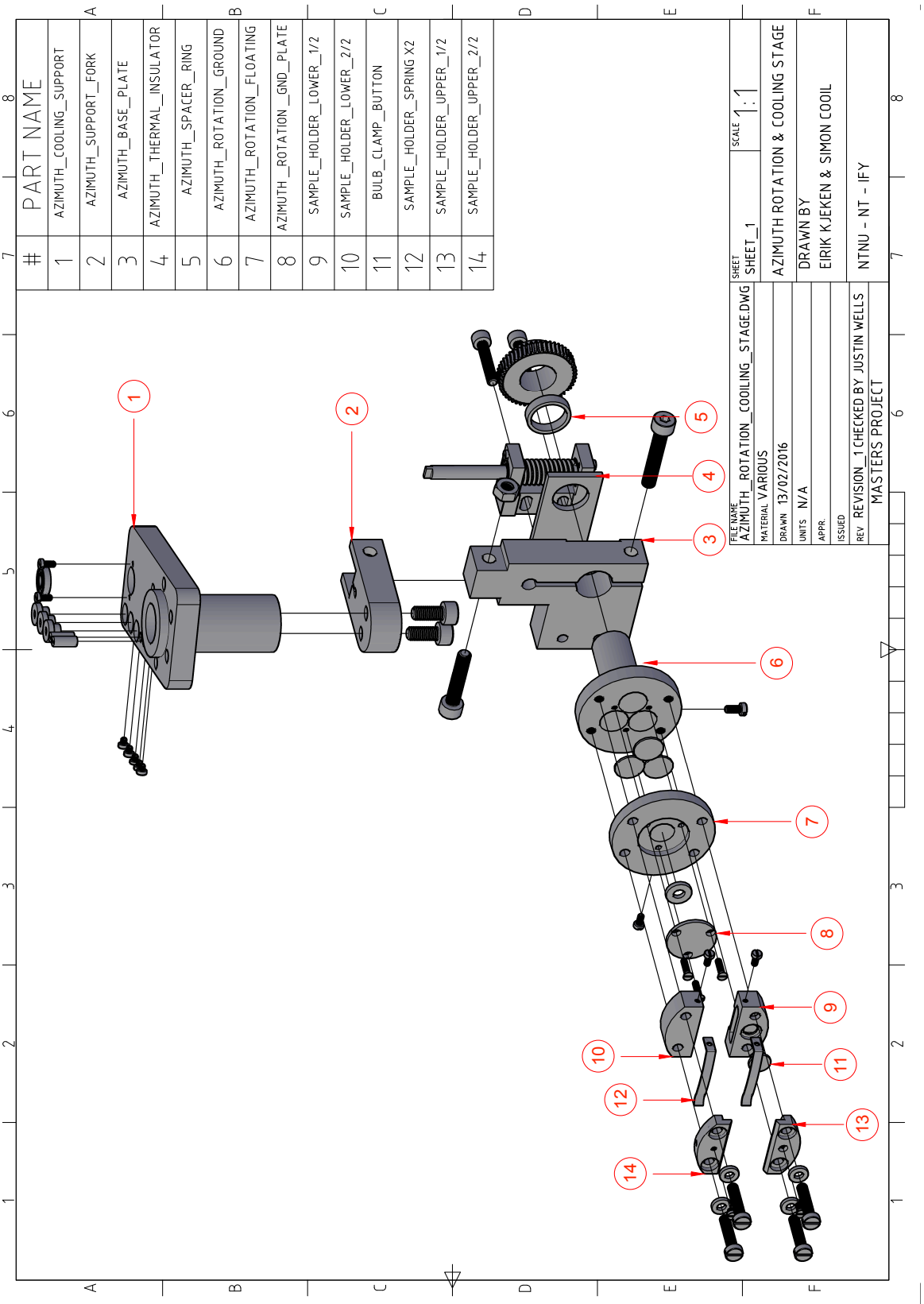


Figure 14: Exploded view of the sample stage design with the manufactured components numbered and named.

### 4.2.1 The Cooling Support

The Cooling support is labeled as number 1 in the exploded view, and is the main source of temperature loss when the sample is cooled. The cooling support acts as the anchor point of the manipulator to the coaxial cryostat stretching out of the chamber through to the different drives that allows for interaction. Liquid nitrogen will be pumped through the cryostat into the hollow pipe protruding from the cooling support. This hollow pipe will act as a reservoir for the liquid nitrogen, allowing it to cool down the cooling support. Thermal conductivity will in turn cool down the rest of the manipulator and eventually the sample itself.

In addition to its role in cooling, the cooling support also acts as a support for different wires and shafts connected to the manipulator. The shaft connected to the worm screw driving the azimuthal rotation passes through a bearing in order to ensure smooth rotation without excessive strain on the shaft. Different wires pass trough holes drilled in the cooling support. To ensure electrical and thermal insulation the holes are lined with small ceramic washers ($Al_2O_3$).

The usual approach to ensure high vacuum seals between connecting pipes is to employ the use of copper gaskets. The inside of the connecting flanges are lined with teeth that bite into the soft copper when tightened, ensuring a tight seal. These gaskets have to be replaced each time the seal is loosened. Since the manipulator is expected to be loosened few times in its lifetime, the cooling support has an "integrated" gasket in the form a protruding ring where the coaxial pipe connects to the cooling support. This ring will act as a gasket, and is estimated to be functional for at least three separate disconnections.

The cooling support is fully made of Oxygen-Free High Thermal Conductivity Copper (OFHC). Copper is ideal for UHV conditions as it is both electrically and thermally conductive while still being stable and rigid enough to minimize offsets caused by expansion and subtractions with temperature. Since copper is naturally oxidized in contact with air, special oxygen free copper was ordered to ensure that oxygen would not evaporate and contaminate the measurements as soon as the sample was heated. Unless specifically stated, all the parts in the manipulator is made from oxygen free copper.

### 4.2.2 The Azimuth Support Fork

Labeled as number 2 on the exploded view, this part acts as a connector between the cooling support and the base plate. Its necessity springs from the fact that the manipulator has to ideally rotate around the $\theta$ axis with the sample lying exactly in the centre of rotation [17]. That is, a rotation around $\theta$ will keep the centre of the sample in the same

spatial coordinates. Since the rotation stage of the manipulator requires a certain height, the azimuth support fork acts as a step down to compensate for this.

### 4.2.3 The Azimuth Base Plate

As the name suggests, this part acts as a base for the entire rotating structure of the manipulator. On its underside sits the worm screw responsible for driving the azimuthal rotation. The orientation of the worm screw is with the rotating shaft parallel to the main support shaft. This was done in order to avoid the use of bevel gears. An extra gear could potentially be a source of backlash between rotation of the sample and the drive manually rotated on the outside of the chamber.

### 4.2.4 Azimuth Thermal Insulator

This component acts as thermal insulation between the worm screw and the rest of the manipulator. This was done in order to maximize the efficiency of the cooling system by limiting the total material to be cooled. The insulator plate is made of a ceramic material called Macor®. The material was chosen for its insulating properties while still being suitable for machining by non specialist ceramic tools such as carbide drills.

### 4.2.5 Azimuth Spacer Ring

This ring is simply a stainless steel ring designed to sit between the main gear on the rotation stage and the base plate. Its purpose is to bring the gear to the appropriate height to smoothly interlock with the worm gear.

### 4.2.6 Azimuth Rotation Stage part 1 - Ground

The component marked as number 6 on the exploded view is the bottom part of the rotation stage. It features a shaft that goes through the base plate and connects to the worm screw through the gear that sits atop the spacer ring. To reduce the total weight of the manipulator, this shaft is hollowed out. This is done to minimize drooping caused by load on the coaxial cryostat shaft that would lead to offsets from the ideal position of the sample.

The component also features grooves fitted to three circular windows. These windows are designed to electrically insulate the component from the rest of the rotation stage. However, the components still need to be thermally conductive. To achieve this, the windows are made of sapphire, as it is one of the few materials that are electrically insulating while still being thermally conductive. Another suitable choice for material would be diamond, which is slightly more thermally conductive than sapphire. The difference in price is however far larger than the gain in thermal conductivity, so the final decision fell on sapphire.

The windows were purchased from Edmund Optics.

Finally, this part has a screw designed to hold a wire. This wire will be connected to ground, grounding the whole component and in turn everything it is in metallic contact with.

### 4.2.7 Azimuth Rotation Stage part 2 - Floating Potential

The components marked as 7 and 8 make up the rest of the mechanism for floating the sample. Part number 7, dubbed the floating plate, has a screw to hold a wire similar to part number 6. This wire can be connected to a voltage, inducing a potential difference between the two parts. All the rest of the parts of the rotation stage will be put at this potential through contact, effectively putting the sample at a potential. In order to achieve an electric field in the direction of the sample, part number 7 has a circular titanium plate that connects to the grounded base of the rotation stage. The plate is electrically connected to ground through the screws, but remains insulated to the rest of the rotation stage by a ceramic washer between the titanium plate and the floating plate.

### 4.2.8 Azimuth rotation stage part 3 - Sample Holder

All the rest of the components make up the part of the rotation stage that holds the sample. The sample will be clamped between parts 9 & 10 and parts 13 & 14. Part 12 marks springs made by molybdenum designed to push the sample up against the roof of parts 13 & 14. Parts 9 & 10 also acts to raise the sample up from the grounding plate, making room for the light bulb filament that will provide the electrons for e-beam heating. Component number 9 is hollowed out for this purpose, and fitted with a small button (labeled as 11). The button can be pushed downward by a screw to clamp the bulb in place. The bulb sits directly in the electric field between the ground plate and the sample. Component number 10 will be the connection point for the thermocouple. The parts features additional screws designed to clamp the wires to the bulb and the thermocouple. In order to keep the floating part of the rotation stage electrically isolated from the grounded part, the four screws clamping them together sits on ceramic washers. Furthermore, the thread has been filed down on the sections of these screws that pass through the floating parts. This was done to ensure that the screws are not in electrical contact with the floating part of the rotation stage.

### 4.2.9 The Screws

All photoemission spectroscopy techniques are sensitive to electrical and magnetic fields, as the presence of such fields can affect the photoelectrons as they exit the sample. To reduce the amount of induced magnetic fields from the metal in the screws, the decision

was made to make all the screws out of titanium. Titanium has low magnetic permiability, minimizing the strength of their magnetic fields. Additionally, titanium has fairly low electrical and thermal conductivity, making it an ideal metal for UHV conditions [18].

The sample stage is also designed to prevent any air being trapped in pockets in the copper. To ensure this, all the holes for screws were either drilled all the way through its component, or a "breathing hole" was drilled to ensure that the air can escape.

### 4.2.10 Azimuth Rotation and Rotation Backlash

The azimuth rotation is transmitted from the drive to the sample stage through a rotating shaft spanning the length of the manipulator. The shaft is supported by a custom made support connected to the cryostat (see Appendix I for model). Rotating the drive situated at the multiport adaptor will rotate the entire shaft. The shaft is connected to the worm screw on the sample stage, which in turns is connected to the gear on the rotation stage. Whenever there is a connection in such an arrangement a certain amount of backlash will occur, meaning that a percentage of the initial rotation will be "lost" due to imperfections in the mechanisms, such as slipping between interlocking parts. To minimize the backlash, the shafts were designed to have as few connections as possible. A direct connection from the worm screw to the drive was not possible due to collisions within the drives. Special flex couplings were donated by Ruland specifically designed to minimize rotation backlash when coupling shafts. The teeth on the rotation stage gear are also rounded to achieve smooth interlocking contact with the worm screw.

### 4.2.11 Gold Plating

In order to maximize thermal conductivity, the possibility of gold plating the copper parts of the manipulator has been investigated. Gold is softer than copper, resulting in better contact for thermal conductivity once the manipulator is assembled. Gold also has a smooth surface and hence a smaller surface area, resulting in less heat loss to the environment. Additionally, the smoother surface will give less degassing from "sharp" edges, making the manipulator better suited for UHV conditions. As of the time of writing, the possibility of gold plating is still being investigated.

# 5 Additional Upgrades

This chapter will presents the additional upgrades that are under way to improve the capabilities for ARPES measurements. All of the components mentioned here are manufactured by companies outside of NTNU, so the focus will be on the motivation behind the upgrades rather than the design. The two major upgrades beside the new manipulator is a new X-ray gun, and a new 2D detector.

## 5.1 The X-ray Gun

As previously mentioned, low energy X-rays are desired when examining the electronic structures of the valence band with ARPES. There is however issues with low X-ray energies. The lower the energies of the photoelectrons, the more susceptible they are to disturbances by magnetic fields in the chamber. The chamber in the lab at NTNU is made of stainless steel, which has a relatively high magnetic permiability. The earth's magnetic field will induce magnetic fields in the stainless steel that can disturb the measurements. A compromise is needed; low enough photon energy to excite electrons from the valence band, but not so low that the measurements are too disturbed by magnetic fields. As a reference, typical energies supplied by beamlines designed for ARPES are in the range of around ten eV to a couple hundred eV [19] [20].

One approach that was pursued was to examine if the $K_\alpha$ line from the oxygen on the magnesium anode could be used. Oxygen has a $K_\alpha$ energy of about 500 eV [21], roughly in the right neighbourhood for ARPES. Although a lower X-ray energy is optimal, it is still closer to the desired energy range than the Mg and Al anode energies. The relative intensity from the Mg $K_\alpha$ and the O $K_\alpha$ vary with anode voltage, and several XPS spectra were collected from the same Iridium(111) sample varying the anode voltage. By comparing the areas of peaks from the same core level in the sample excited by the different X-ray lines, the anode voltage maximizing the intensity of the O $K_\alpha$ line can be determined. The results are shown in Figure 15. Comparing the intensity of the peaks over different anode voltages gave $\approx 8kV$ as the best voltage for using the O $K_\alpha$ line.

The use of the O $K_\alpha$ line was however not deemed an ideal solution since the intensity is relatively low and the radiation from the Al will always be present, polluting the measurements. A decision was taken to order a new X-ray gun, identical to the one currently in use, and coat the anode with a new metal with an excitation line in the appropriate energy range. The likely candidate for the coating is yttrium, with a main excitation line of 132.3

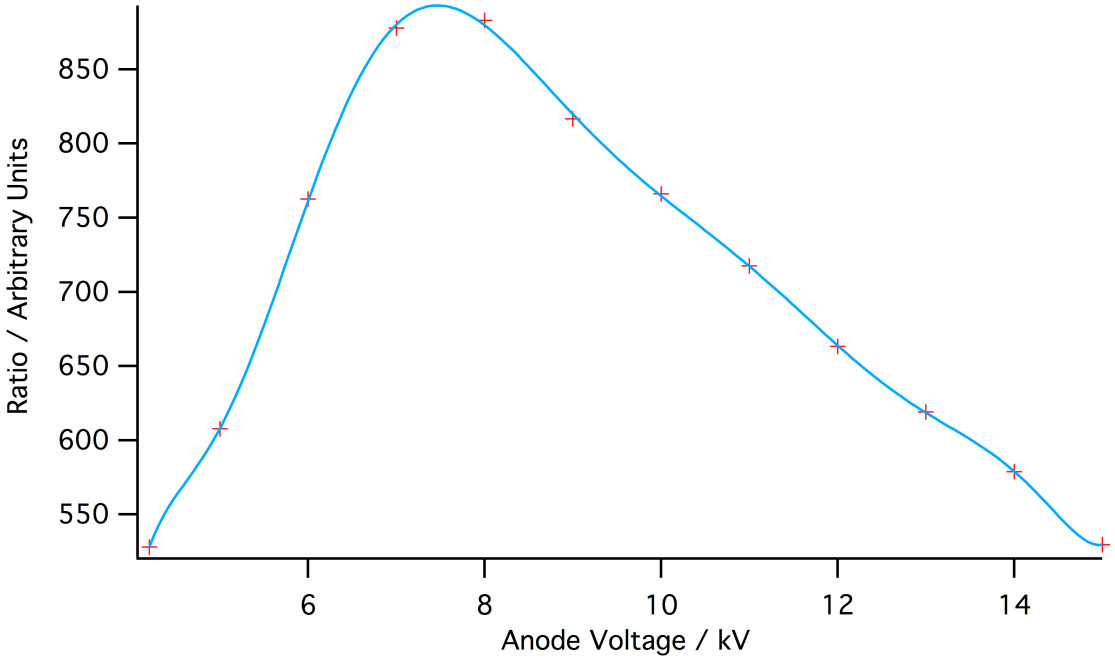


Figure 15: Graph showing the ratio between the areas of an Ir 4f core level excited by oxygen and magnesium $K_\alpha$ lines, for varying anode voltage. The graph between points is a polynomial fit to illustrate the trend. The data has been normalized for flux and power. The peak at around 8 kV gives the best anode voltage for using the oxygen $K_\alpha$ line.

eV [22]. This project will start during the summer of 2016, unfortunately too late to make it into this thesis.

## 5.2 The detector

The 1D detector will be swapped for a new 2D CCD detector purchased from SPECS. The installation and upgrade will all be handled by SPECS. The addition of a 2D detector will greatly enhance the capabilities of the chamber, as ARPES measurements can now be taken over much larger angles (up to ±15°, covering 30° in WAM), drastically cutting down time spent on gathering data for each measurement. The advantages of a 2D detector has already been demonstrated (recall Figure 10), and the combination of a 5-axis manipulator with a 2D detector will greatly increase the quality and efficiency of ARPES measurements.

# 6 Future improvements

This section will detail additional improvements to the chamber that could be implemented in the future.

## 6.1 The Chamber Material

The current chamber is made of stainless steel, and the consequences of the magnetic fields that arise in stainless steel have already been discussed. One possibility to avoid the problem altogether is to make a new chamber out of another material. Mu-metal is a likely candidate, a nickel-iron alloy made specifically to avoid inducing magnetic fields [23]. Refitting the lab with a new chamber is certainly a daunting task, but it should be within the realm of possibility provided a budget that allows for such an upgrade.

## 6.2 A 6-axis Manipulator

This thesis has revolved around the design of a 5-axis manipulator. Introducing the possibility for rotations around a final axis ("tilting" the sample) would certainly improve upon the current design. Tilting the sample would allow for compensation of drooping of the cryostat arm, and orienting the sample for measurements of specific surfaces of the Brillouin zone [24]. The size of the drives on the 5-axis manipulator are already on the brink of being too large for the chamber, so a new 6-axis manipulator would need to be accompanied with an expansion of the table around the chamber and a new way of supporting the drives. Provided the space and budget, it should however not be an impossible task.

## 6.3 The X-ray gun

The problems with spot size and polychromatic radiation have been discussed in previous chapters, and the problem could be addressed by the inclusion of a monochromator. A monochromator filters out a narrow band of the desired radiation from the spectrum through clever manipulation of prisms or grates (to exploit refraction or diffraction respectively [4]). The monochromator could ideally be installed to simultaneously focus the radiation to a spot, dealing with the issues of spot size in addition to the polychromatic radiation. The drawback of a monochromator is that a large number of photons are lost through the filtering process, and the result is a severe decrease in intensity once the filtered radiation reaches the sample. This would imply increased collection times for each measurement. Further investigation is needed to validate if the compromise for quality over time is a worthwhile investment.

# 7 Concluding remarks

This thesis has attempted to give an outline of the design of a 5-axis manipulator for use in ARPES. The focus has been on addressing the specific challenges involved in doing ARPES, and to give the reader an understanding of what is physically demanded of the equipment for these kinds of measurements. The theory section has also been written in the same spirit, and the focus was not on the intricate mathematical detail but rather on giving the reader an appreciation of the problems the manipulator has to face. The reader is encouraged to consult references for further information and technical rigor.

Sadly, the manipulator will not be finished for testing by the time this thesis reaches its deadline. If everything works as intended, the manipulator should serve as a significant upgrade to the one currently in use. Although the manipulator is tailored to suit the UHV chamber at NTNU, some of the design solutions (specifically the float/ground mechanism) are applicable to a range of other scenarios and could be recycled elsewhere. It is the author's hope that he can, through future work done possible by the new manipulator, contribute ever so slightly to the expanding collection of knowledge that is science.

# List of Tables

# Bibliography


[1] Graham Farmelo. *Great Equations of Modern Science*. London and New York: Granta Books, 2002.

[2] Kai Siegbahn. Electron spectroscopy for chemical analysis (ESCA). *Philosophical Transactions of the Royal Society of London. Series A, Mathematical and Physical Sciences*, 268(1184):33–57, 1970.

[3] Kai Siegbahn, Ulrik Gelius, Hans Siegbahn, and Erik Olson. Angular distribution of electrons in ESCA spectra from a single crystal. *Physica Scripta*, 1(5-6):272, 1970.

[4] Jens Als-Nielsen and Des McMorrow. *Elements of modern X-ray physics*. John Wiley & Sons, 2011.

[5] Simon Phillip. Controlling the Epitaxial Growth of Graphene On Diamond Surfaces. *Ph.d thesis, Aberystwyth University*.

[6] Rene Van Grieken and Andrzej Markowicz. *Handbook of X-ray Spectrometry*. CRC Press, 2001.

[7] MO Krause and JG Ferreira. K X-ray emission spectra of Mg and Al. *Journal of Physics B: Atomic and Molecular Physics*, 8(12):2007, 1975.

[8] Andrea Damascelli. Probing the electronic structure of complex systems by ARPES. *Physica Scripta*, 2004(T109):61, 2004.

[9] D Roy and D Tremblay. Design of electron spectrometers. *Reports on Progress in Physics*, 53(12):1621, 1990.

[10] PP Manning, NJ Clague, IW Kirkman, FM Quinn, and PJ Hicks. A fast and flexible multichannel electron detector with parallel readout for photoelectron spectroscopy. *Nuclear Instruments and Methods in Physics Research Section A: Accelerators, Spectrometers, Detectors and Associated Equipment*, 392(1):345–348, 1997.

[11] Joseph Ladislas Wiza. Microchannel plate detectors. *Nuclear Instruments and Methods*, 162(1):587–601, 1979.

[12] X-ray source XR 50. http://www.specs.de/cms/front_content.php?idcat=118. last visited 30/05-16.

[13] JJ Yeh and I Lindau. Atomic subshell photoionization cross sections and asymmetry parameters: $1 \leqslant Z \leqslant 103$. *Atomic data and nuclear data tables*, 32(1):1–155, 1985.

[14] SPECS Phoibos 100/150. http://www.specs.de/cms/front_content.php?idart=122. last visited 30/05-16.

[15] Lewvacs websites with downloadable catalouge. http://lewvac.com/index_files/Page1059.htm, 2016. Last visited 26/05-16.

[16] A Goldmann and R Matzdorf. Temperature effects in angle-resolved photoemission spectra from metals. *Progress in surface science*, 42(1):331–350, 1993.

[17] Bum Joon Kim, Hyeong-Do Kim, Deok-Yong Cho, Myongjin Kim, S-J Oh, and Changyoung Kim. Stable five axes cryogenic photoemission manipulator without a differentially pumped rotary feedthrough. *Review of scientific instruments*, 76(6):063910, 2005.

[18] Encyclopedia Britannica titanium. http://global.britannica.com/science/titanium. last visited 08/06-16.

[19] The SGM 3 beamline at ASTRID. http://www.isa.au.dk/facilities/astrid/beamlines/sgm3/sgm3.asp. last visited 27/05-16.

[20] Beamline I4 - short information. https://www.maxlab.lu.se/beamlines/I4. last visited 27/05-16.

[21] X-ray emission lines. http://www.med.harvard.edu/jpnm/physics/refs/xrayemis.html. last visited 27/05-16.

[22] MO Krause. The M$\zeta$ X rays of Y to Rh in photoelectron spectrometry. *Chemical Physics Letters*, 10(1):65–69, 1971.

[23] David Jiles. *Introduction to magnetism and magnetic materials*. CRC press, 2015.

[24] D-J Wang, C-C Chiu, and C-M Cheng. Design of a six-axis cryogenic sample manipulator for angle-resolved photoemission spectroscopy. *Diamond Light Source Proceedings*, 1(MEDSI-6):e9, 2011.

# I Technical Drawings of the Sample Stage

# AZIMUTH ROTATION SAMPLE STAGE

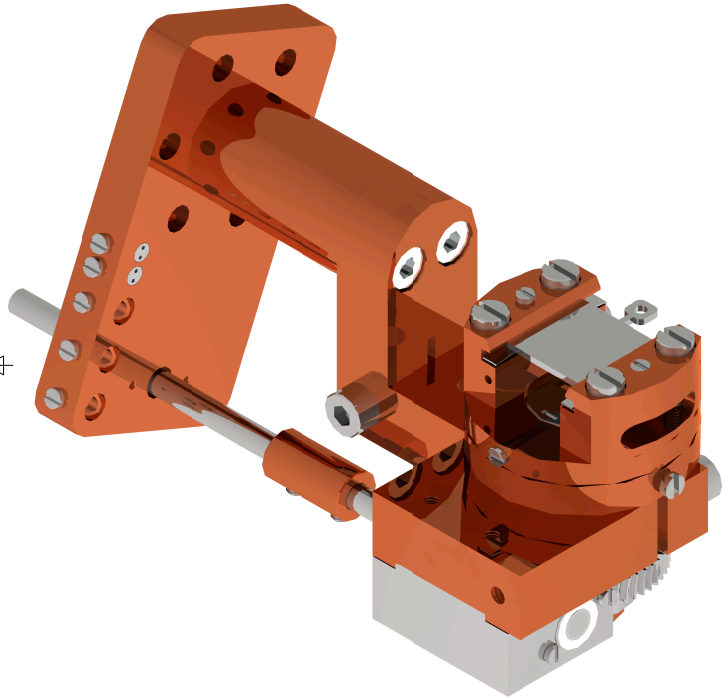

| PART NAME | SHEET NUMBER |
|---|---|
| EXPLODED_VIEW | 1 |
| AZIMUTH_COOLING_SUPPORT | 2 |
| AZIMUTH_SUPPORT_FORK | 3 |
| AZIMUTH_BASE_PLATE | 4 |
| AZIMUTH_THERMAL_INSULATOR | 5 |
| AZIMUTH_SPACER_RING | 6 |
| AZIMUTH_ROTATION_GROUND | 7 |
| AZIMUTH_ROTATION_FLOATING | 8 |
| AZIMUTH _ROTATION _GND_PLATE | 9 |
| SAMPLE_HOLDER_LOWER_1/2 | 10 |
| SAMPLE_HOLDER_LOWER_2/2 | 11 |
| BULB_CLAMP_BUTTON | 12 |
| SAMPLE_HOLDER_SPRING X2 | 13 |
| SAMPLE_HOLDER_UPPER_1/2 | 14 |
| SAMPLE_HOLDER_UPPER_2/2 | 15 |
| Z_DRIVE_SUPPORT | 16 |
| LIST_OF_SCREWS | 17 |
| CUT_DIAGRAM_1 | 18 |
| CUT_DIAGRAM_2 | 19 |

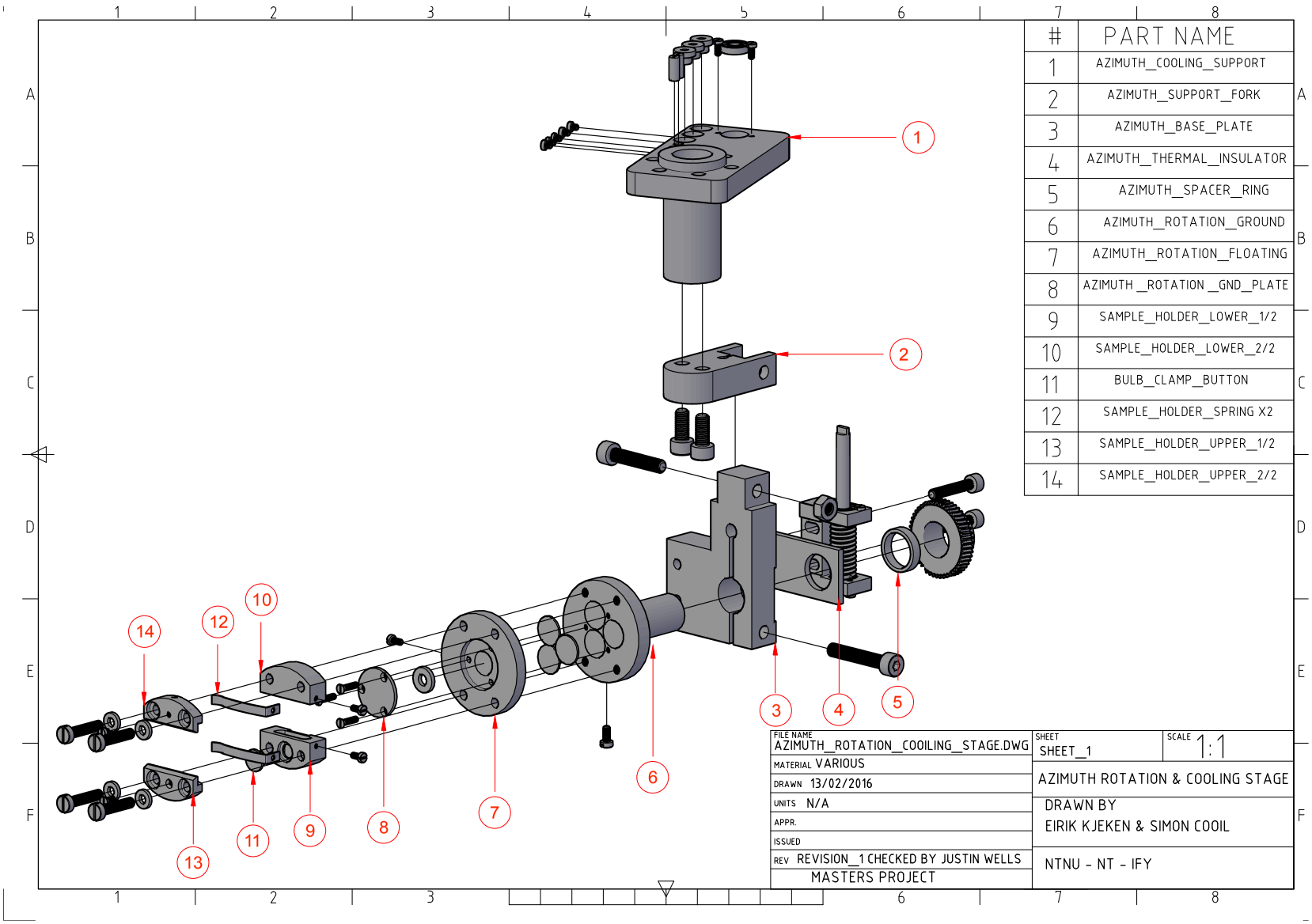


| # | PART NAME |
|---|---|
| 1 | AZIMUTH_COOLING_SUPPORT |
| 2 | AZIMUTH_SUPPORT_FORK |
| 3 | AZIMUTH_BASE_PLATE |
| 4 | AZIMUTH_THERMAL_INSULATOR |
| 5 | AZIMUTH_SPACER_RING |
| 6 | AZIMUTH_ROTATION_GROUND |
| 7 | AZIMUTH_ROTATION_FLOATING |
| 8 | AZIMUTH _ROTATION _GND_PLATE |
| 9 | SAMPLE_HOLDER_LOWER_1/2 |
| 10 | SAMPLE_HOLDER_LOWER_2/2 |
| 11 | BULB_CLAMP_BUTTON |
| 12 | SAMPLE_HOLDER_SPRING X2 |
| 13 | SAMPLE_HOLDER_UPPER_1/2 |
| 14 | SAMPLE_HOLDER_UPPER_2/2 |

FILE NAME AZIMUTH_ROTATION_COOILING_STAGE.DWG
MATERIAL VARIOUS
DRAWN 13/02/2016
UNITS N/A
APPR.
ISSUED
REV REVISION_1 CHECKED BY JUSTIN WELLS
MASTERS PROJECT

SHEET SHEET_1
SCALE 1:1

AZIMUTH ROTATION & COOLING STAGE

DRAWN BY
EIRIK KJEKEN & SIMON COOIL

NTNU - NT - IFY

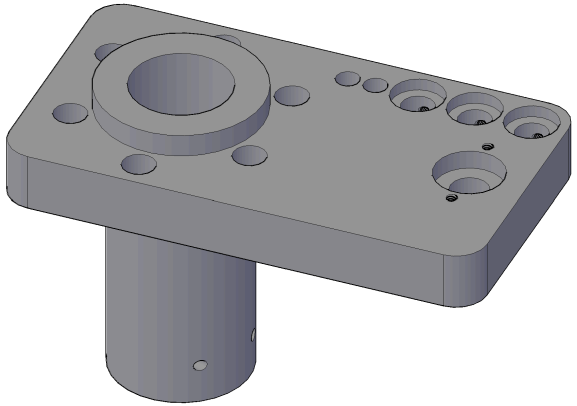

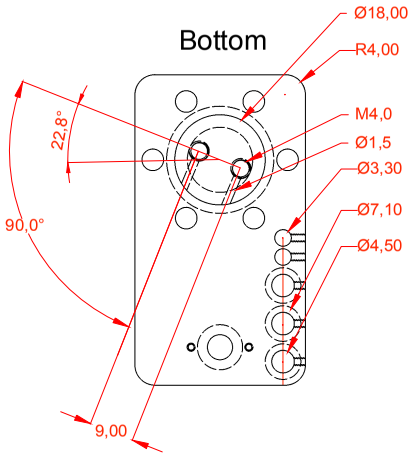


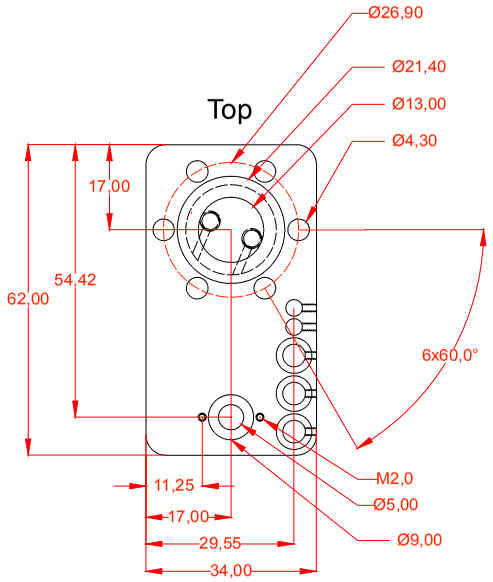


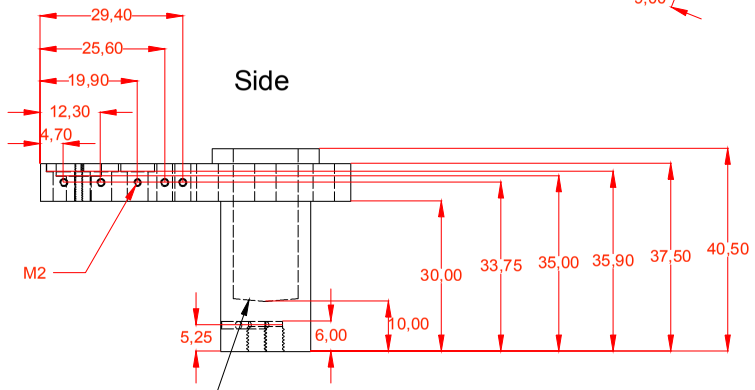


Note: dimensions on drill bit not critical

| | | | |
|---|---|---|---|
| FILE NAME AZIMUTH_COOILING_SUPPORT.DWG | | SHEET SHEET_2 | SCALE 1.25:1 |
| MATERIAL OXYGEN-FREE COPPER | | AZIMUTH COOLING SUPPORT | |
| DRAWN 05/02/2016 | | DRAWN BY<br>EIRIK KJEKEN & SIMON COOIL | |
| UNITS MM | | | |
| APPR. | | | |
| ISSUED | | | |
| REV REVISION_1 CHECKED BY JUSTIN WELLS | | NTNU - NT - IFY | |
| CONTRACT NO MASTERS PROJECT | | | |

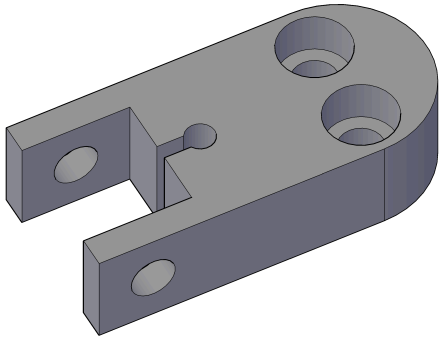

Bottom

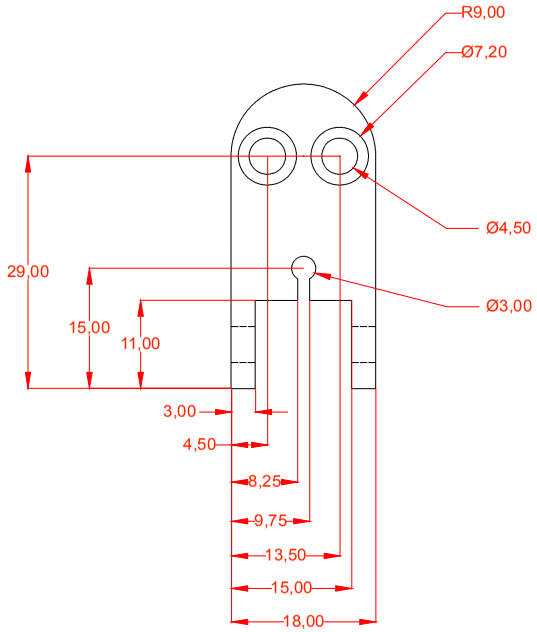


Side

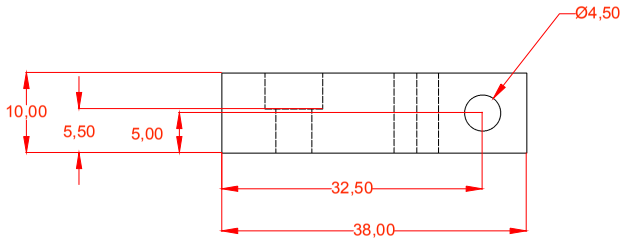


| | | |
|---|---|---|
| FILE NAME MANIPULATOR_DOGLEG.DWG | SHEET SHEET_3 | SCALE 2:1 |
| MATERIAL OXYGEN-FREE COPPER | AZIMUTH SUPPORT FORK | |
| DRAWN 08/02/2016 | DRAWN BY<br>EIRIK KJEKEN & SIMON COOIL | |
| UNITS MM | | |
| APPR. | | |
| ISSUED | | |
| REV REVISION_1 CHECKED BY JUSTIN WELLS | NTNU - NT - IFY | |
| CONTRACT NO MASTERS PROJECT | | |

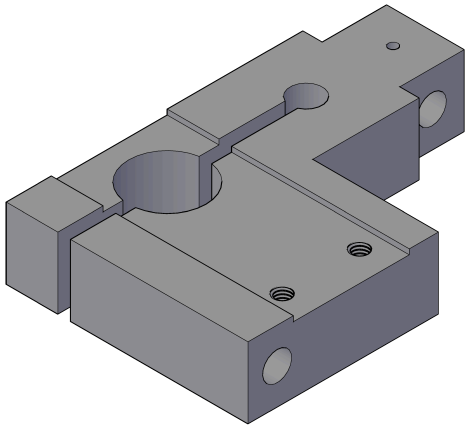

Back

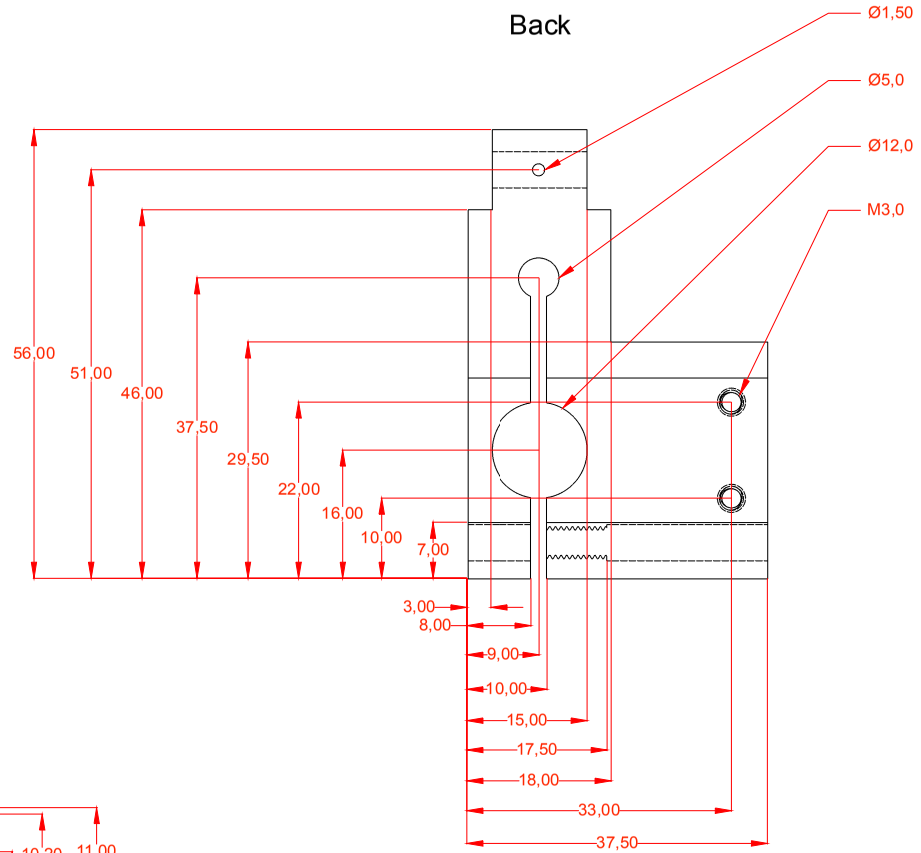


Side

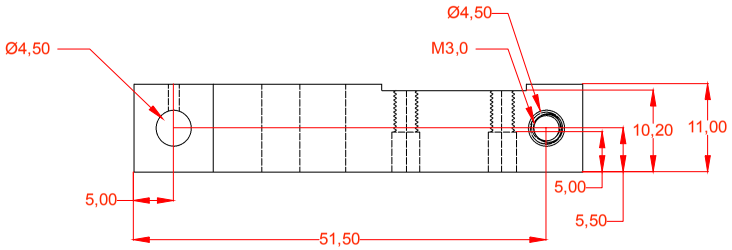


| | | |
|---|---|---|
| FILE NAME MANIPULATOR_BASEPLATE.DWG | SHEET SHEET_4 | SCALE 2:1 |
| MATERIAL OXYGEN-FREE COPPER | AZIMUTH BASE PLATE | |
| DRAWN 10/02/2016 | DRAWN BY<br>EIRIK KJEKEN & SIMON COOIL | |
| UNITS MM | | |
| APPR. | | |
| ISSUED | | |
| REV REVISION_1 CHECKED BY JUSTIN WELLS | NTNU - NT - IFY | |
| CONTRACT NO MASTERS PROJECT | | |

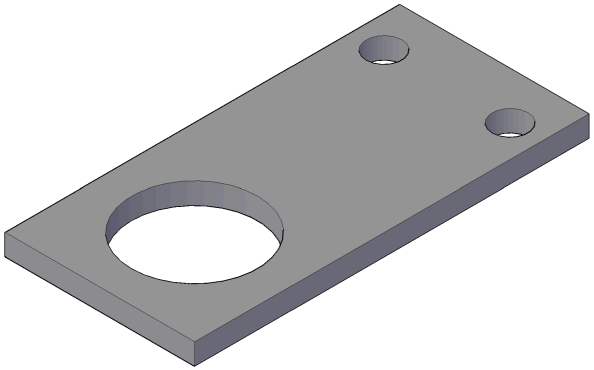

Top

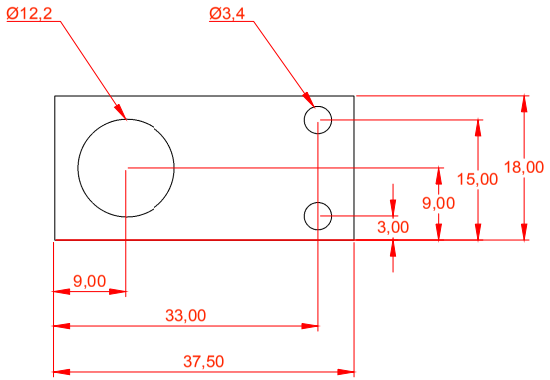


Side

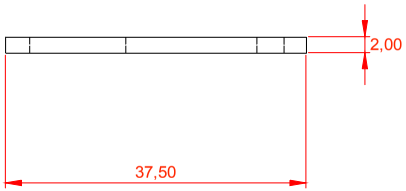


| | | |
|---|---|---|
| FILE NAME BASE_ISOLATION_PLATE.DWG | SHEET SHEET_5 | SCALE 2:1 |
| MATERIAL MACOR | BASE THERMAL ISOLATION PLATE | |
| DRAWN 11/02/2016 | DRAWN BY<br>EIRIK KJEKEN & SIMON COOIL | |
| UNITS MM | | |
| APPR. | | |
| ISSUED | | |
| REV REVISION_1 CHECKED BY JUSTIN WELLS | NTNU - NT - IFY | |
| CONTRACT NO MASTERS PROJECT | | |

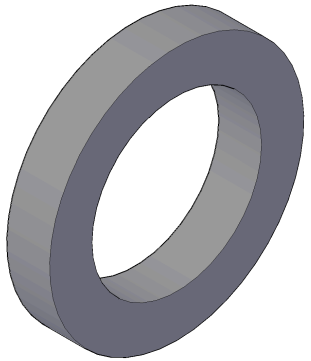

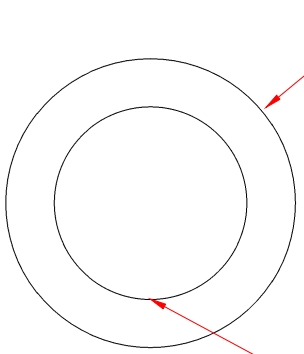



| | | |
|---|---|---|
| FILE NAME AZIMUTH_SPACER_RING.DWG | SHEET SHEET_6 | SCALE 4:1 |
| MATERIAL STAINLESS STEEL | AZIMUTH SPACER RING | |
| DRAWN 15/02/2016 | DRAWN BY<br>EIRIK KJEKEN & SIMON COOIL | |
| UNITS MM | | |
| APPR. | | |
| ISSUED | | |
| REV REVISION_1 CHECKED BY JUSTIN WELLS | NTNU - NT - IFY | |
| CONTRACT NO MASTERS PROJECT | | |

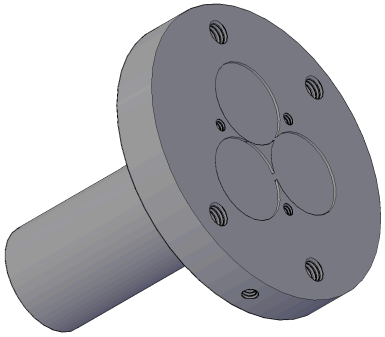

Top

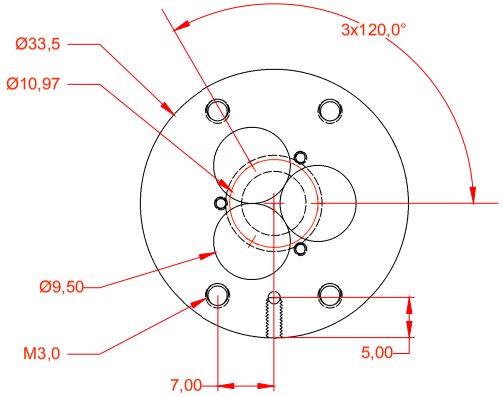


Bottom

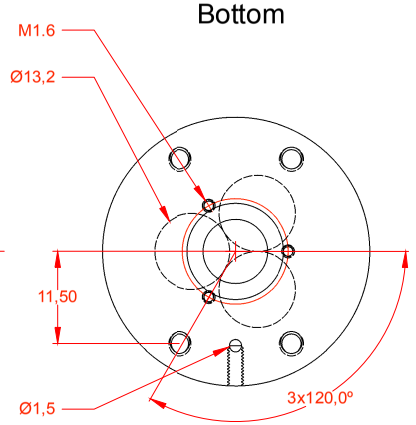


Side

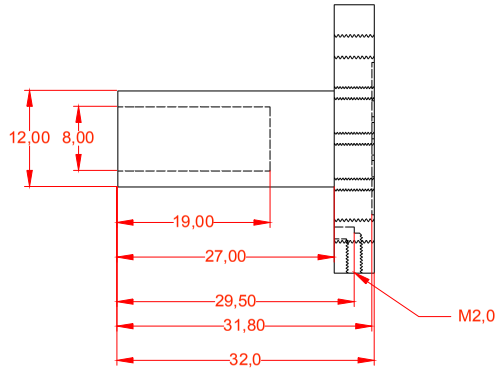


| | | | |
|---|---|---|---|
| FILE NAME ROTATION_STAGE_1.DWG | SHEET SHEET_7 | SCALE 2:1 | |
| MATERIAL OXYGEN-FREE COPPER | AZIMUTH_ROTATION_GROUND | | |
| DRAWN 09/02/2016 | DRAWN BY<br>EIRIK KJEKEN & SIMON COOIL | | |
| UNITS MM | | | |
| APPR. | | | |
| ISSUED | | | |
| REV REVISION_1 CHECKED BY JUSTIN WELLS | NTNU - NT - IFY | | |
| CONTRACT NO MASTERS PROJECT | | | |

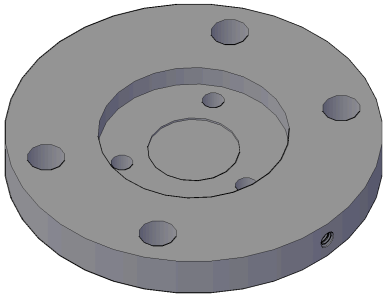

Top

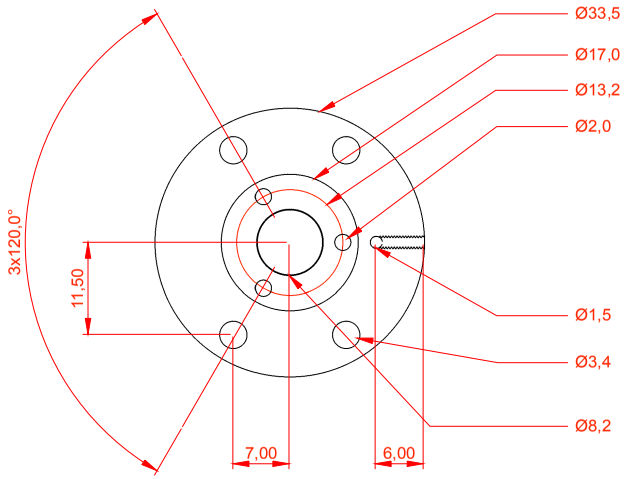


Side

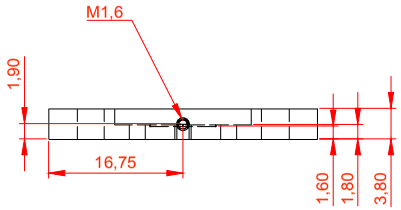


| | | | |
|---|---|---|---|
| FILE NAME ROTATION_STAGE_2.DWG | | SHEET SHEET_8 | SCALE 2:1 |
| MATERIAL OXYGEN-FREE COPPER | | AZIMUTH ROTATION FLOATING | |
| DRAWN 11/02/2016 | | DRAWN BY<br>EIRIK KJEKEN & SIMON COOIL | |
| UNITS MM | | | |
| APPR. | | | |
| ISSUED | | | |
| REV REVISION_1 CHECKED BY JUSTIN WELLS | | NTNU - NT - IFY | |
| CONTRACT NO MASTERS PROJECT | | | |

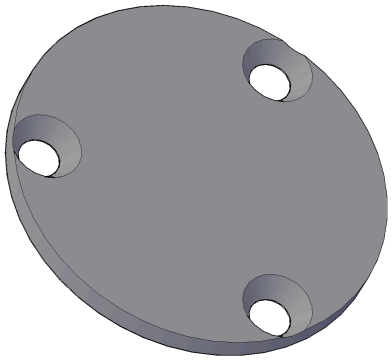

Top

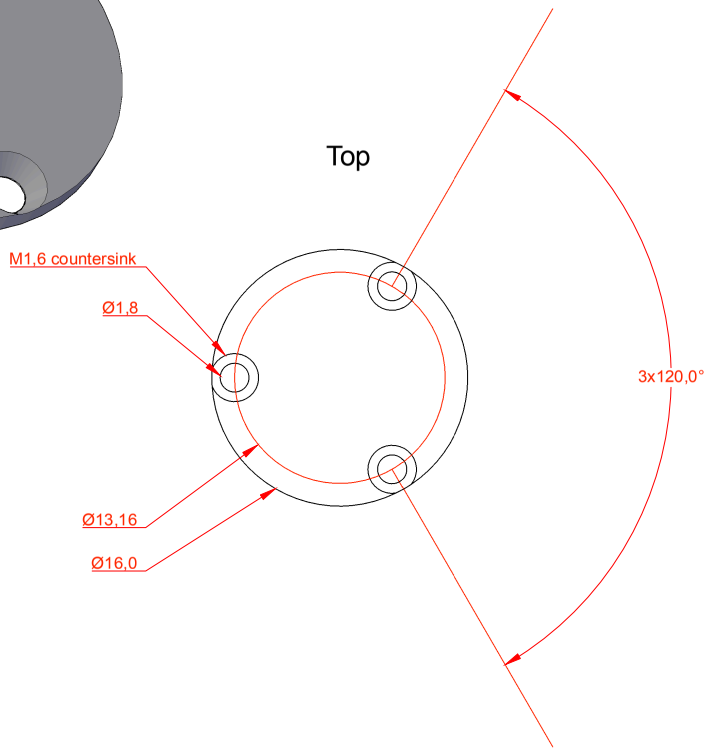


Side

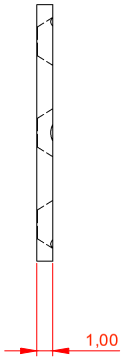


| | | |
|---|---|---|
| FILE NAME ROTATION_STAGE_3.DWG | SHEET SHEET_9 | SCALE 4 : 1 |
| MATERIAL TITANIUM | AZIMUTH ROTATION GND PLATE | |
| DRAWN 11/02/2016 | DRAWN BY<br>EIRIK KJEKEN & SIMON COOIL | |
| UNITS MM | | |
| APPR. | | |
| ISSUED | | |
| REV REVISION_1 CHECKED BY JUSTIN WELLS | NTNU - NT - IFY | |
| CONTRACT NO MASTERS PROJECT | | |

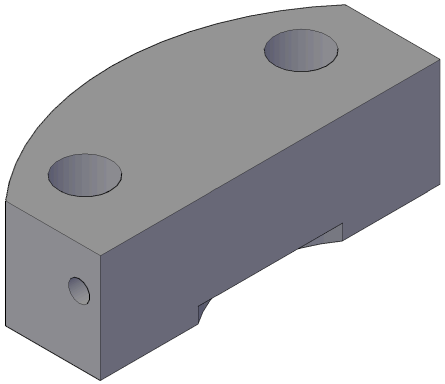

Bottom

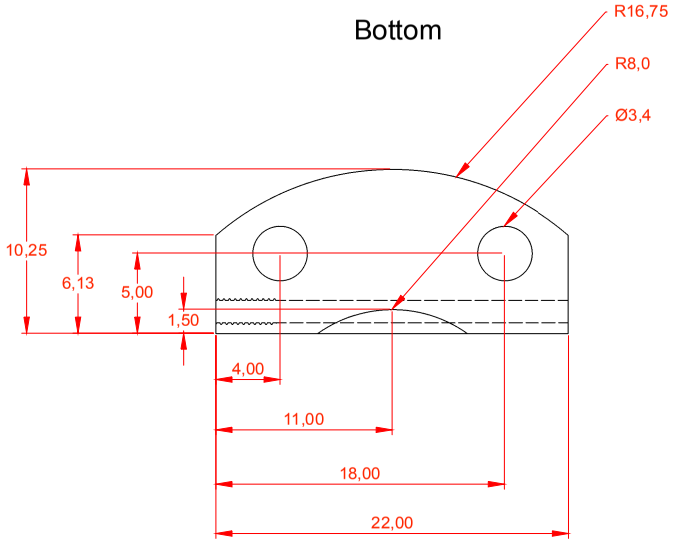


Side

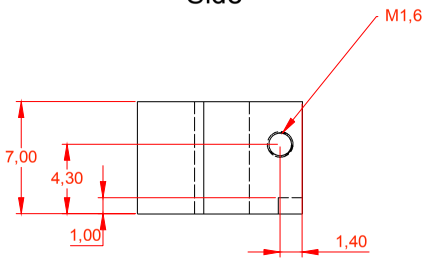


| | | |
|---|---|---|
| FILE NAME ROTATION_STAGE_4.DWG | SHEET SHEET_10 | SCALE 4:1 |
| MATERIAL OXYGEN-FREE COPPER | SAMPLE HOLDER LOWER PART 1/2 | |
| DRAWN 11/02/2016 | DRAWN BY<br>EIRIK KJEKEN & SIMON COOIL | |
| UNITS MM | | |
| APPR. | | |
| ISSUED | | |
| REV REVISION_1 CHECKED BY JUSTIN WELLS | NTNU - NT - IFY | |
| CONTRACT NO MASTERS PROJECT | | |

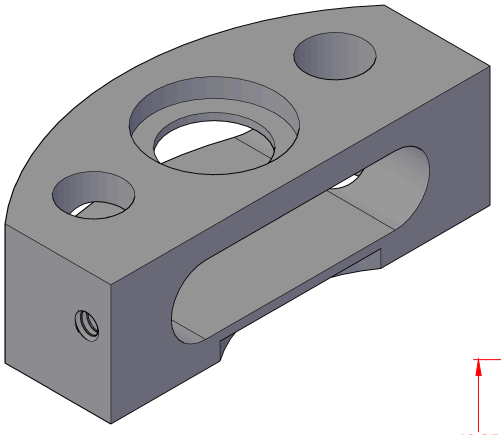

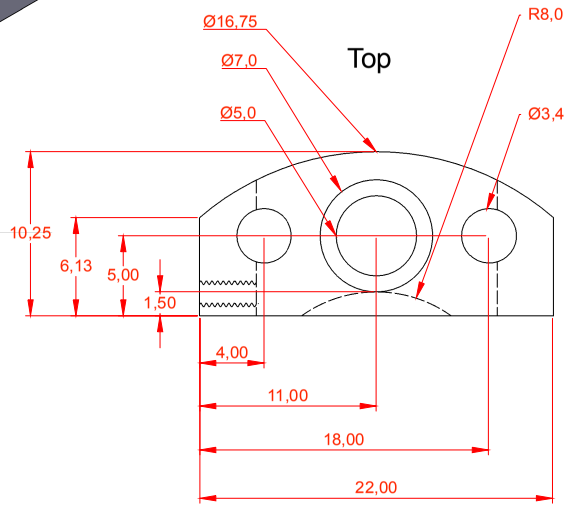


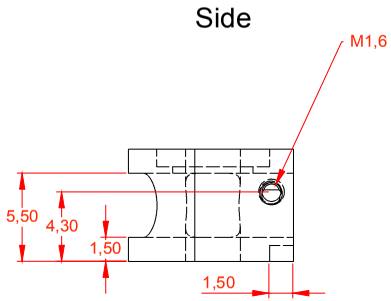


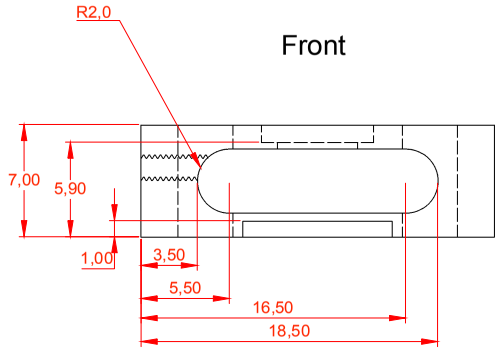


| | | |
|---|---|---|
| FILE NAME ROTATION_STAGE_5.DWG | SHEET SHEET_11 | SCALE 4:1 |
| MATERIAL OXYGEN-FREE COPPER | SAMPLE HOLDER LOWER PART 2/2 | |
| DRAWN 11/02/2016 | DRAWN BY<br>EIRIK KJEKEN & SIMON COOIL | |
| UNITS MM | | |
| APPR. | | |
| ISSUED | | |
| REV REVISION_1 CHECKED BY JUSTIN WELLS | NTNU - NT - IFY | |
| CONTRACT NO MASTERS PROJECT | | |

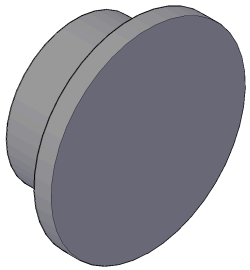

Bottom

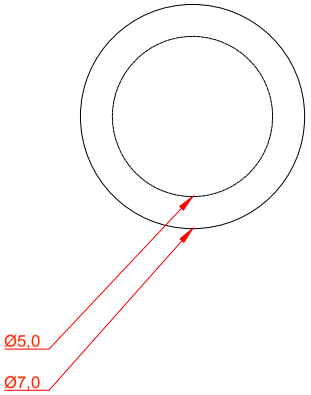


Side

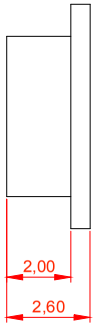


| | | | |
|---|---|---|---|
| FILE NAME ROTATION_STAGE_6.DWG | | SHEET SHEET_12 | SCALE 8:1 |
| MATERIAL OXYGEN-FREE COPPER | | BULB CLAMP BUTTON | |
| DRAWN 11/02/2016 | | DRAWN BY EIRIK KJEKEN & SIMON COOIL | |
| UNITS MM | | | |
| APPR. | | | |
| ISSUED | | | |
| REV REVISION_1 CHECKED BY JUSTIN WELLS | | NTNU - NT - IFY | |
| CONTRACT NO MASTERS PROJECT | | | |

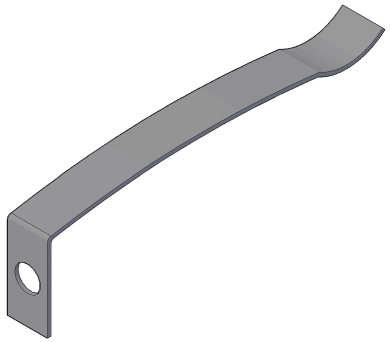

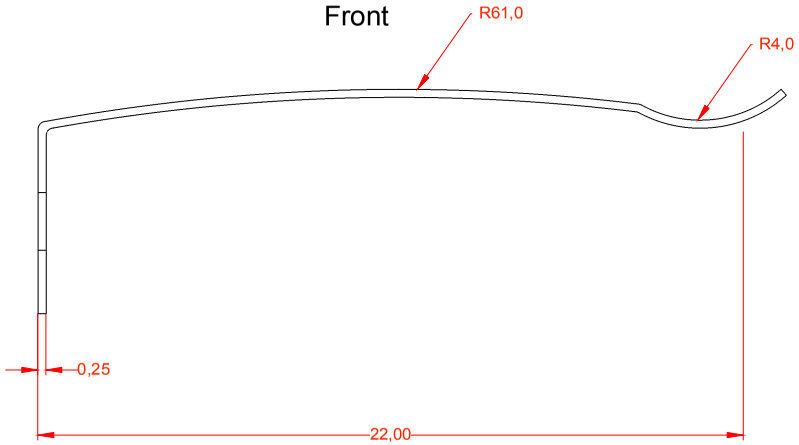


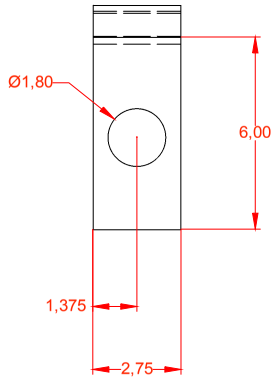


| | | | |
|---|---|---|---|
| FILE NAME ROTATION_STAGE_7.DWG | SHEET SHEET_13 | SCALE 8:1 | |
| MATERIAL ??? | SAMPLE HOLDER SPRING | | |
| DRAWN 11/02/2016 | DRAWN BY EIRIK KJEKEN & SIMON COOIL | | |
| UNITS MM | | | |
| AMOUNT 2X | | | |
| ISSUED | | | |
| REV REVISION_1 CHECKED BY JUSTIN WELLS | NTNU - NT - IFY | | |
| CONTRACT NO MASTERS PROJECT | | | |

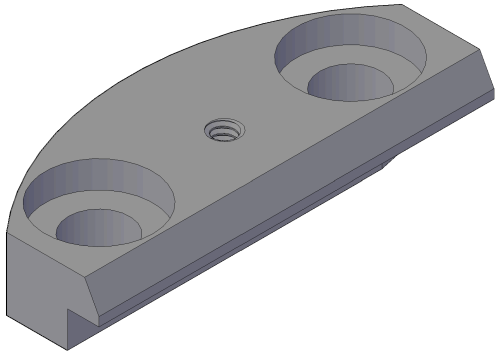

Top

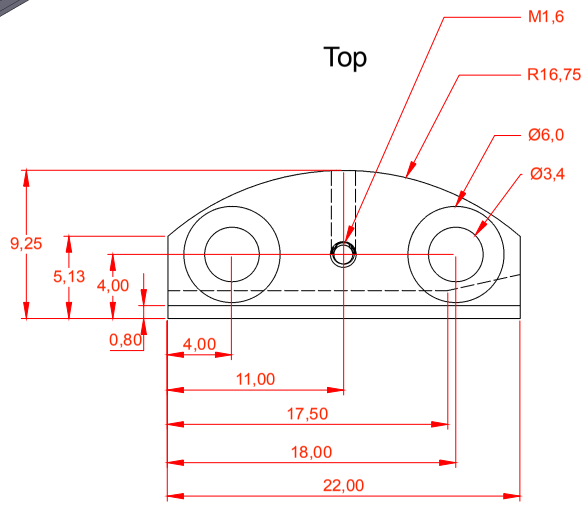


Back

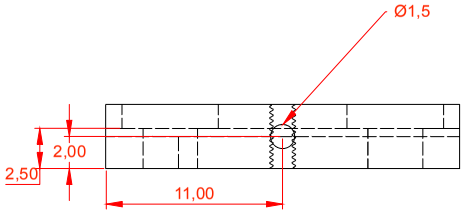


Side

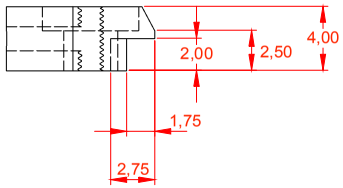


| | | |
|---|---|---|
| FILE NAME ROTATION_STAGE_8.DWG | SHEET SHEET_14 | SCALE 4:1 |
| MATERIAL OXYGEN-FREE COPPER | SAMPLE HOLDER UPPER PART 1/2 | |
| DRAWN 11/02/2016 | DRAWN BY<br>EIRIK KJEKEN & SIMON COOIL | |
| UNITS MM | | |
| APPR. | | |
| ISSUED | | |
| REV REVISION_1 CHECKED BY JUSTIN WELLS | NTNU - NT - IFY | |
| CONTRACT NO MASTERS PROJECT | | |

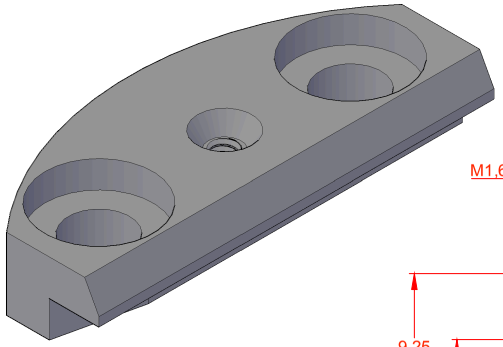

Top

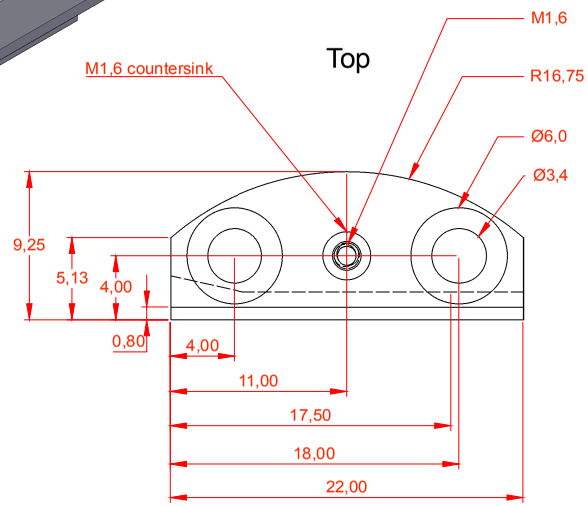


Front

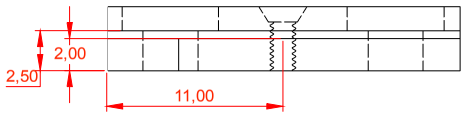


Side

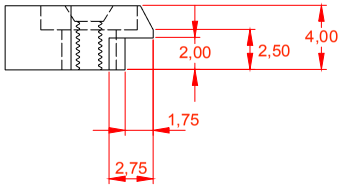


| | | |
|---|---|---|
| FILE NAME ROTATION_STAGE_9.DWG | SHEET SHEET_15 | SCALE 4:1 |
| MATERIAL OXYGEN-FREE COPPER | SAMPLE HOLDER UPPER PART 2/2 | |
| DRAWN 11/02/2016 | DRAWN BY<br>EIRIK KJEKEN & SIMON COOIL | |
| UNITS MM | | |
| APPR. | | |
| ISSUED | | |
| REV REVISION_1 CHECKED BY JUSTIN WELLS | NTNU - NT - IFY | |
| CONTRACT NO MASTERS PROJECT | | |

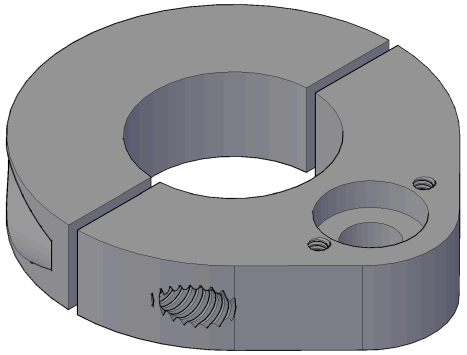

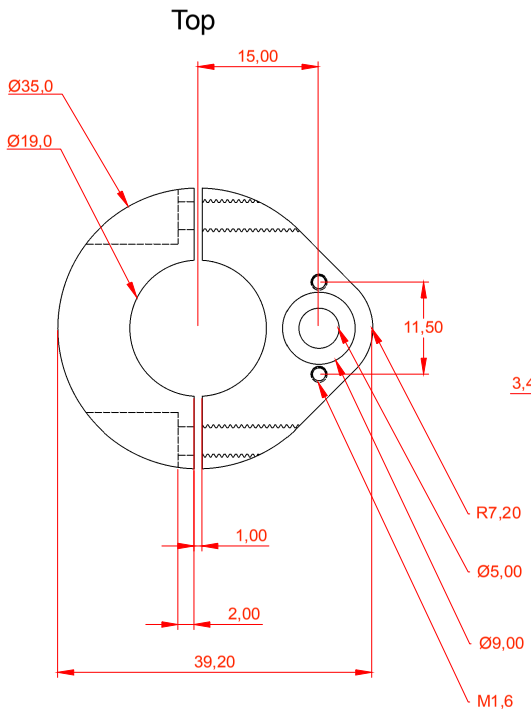


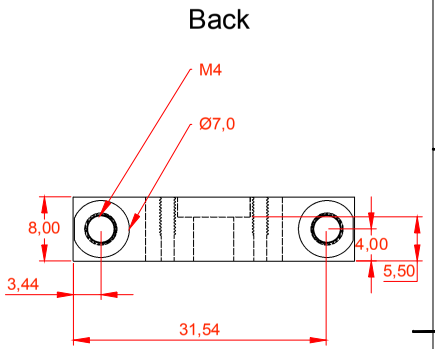


| | | | |
|---|---|---|---|
| FILE NAME Z-DRIVE_SUPPORT.DWG | | SHEET SHEET_16 | SCALE 2:1 |
| MATERIAL STAINLESS STEEL | | Z-DRIVE SUPPORT | |
| DRAWN 24/02/2016 | | DRAWN BY EIRIK KJEKEN & SIMON COOIL | |
| UNITS MM | | | |
| APPR. | | | |
| ISSUED | | | |
| REV REVISION_0 | | NTNU - NT - IFY | |
| MASTERS PROJECT | | | |

# LIST OF SCREWS USED IN ASSEMBLY

Slot fastener

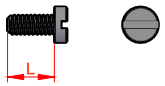


Allen fastener

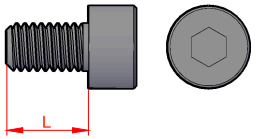


Slot countersirk

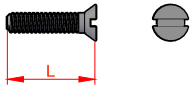


| DIN | SIZE | MATERIAL | L | AMOUNT | HEAD | PURPOSE |
|---|---|---|---|---|---|---|
| 912 | M4 | STAINLESS STEEL | 14.0 | 2 | ALLEN FASTENER | Clamp for Z-drive support |
| 912 | M4 | TITANIUM | 10.0 | 2 | ALLEN FASTENER | Connect dogleg to cooling support |
| 912 | M4 | TITANIUM | 22.0 | 1 + NUT | ALLEN FASTENER | Clamp dogleg to base plate |
| 912 | M4 | TITANIUM | 18.0 | 1 | ALLEN FASTENER | Clamping the rotation stage |
| 912 | M3 | TITANIUM | 16.0 | 2 | ALLEN FASTENER | Connecting wormscrew to base plate |
| 84 | M3 | TITANIUM | 17.0 | 4 | SLOT FASTENER | Connecting rotation stages |
| 84 | M2 | TITANIUM | 6.0 | 4 | SLOT FASTENER | Secure bearings |
| 84 | M2 | TITANIUM | 5.0 | 1 | SLOT FASTENER | Wire clamping rotation stage 1 |
| 963 | M1.6 | TITANIUM | 8.0 | 3 | SLOT COUNTERSINK | Fastening rotation stage isolation plate |
| 84 | M1.6 | TITANIUM | 5.0 | 1 | SLOT FASTENER | Wire clamping rotation stage 2 |
| 84 | M1.6 | TITANIUM | 4.0 | 2 | SLOT FASTENER | Fastening springs |
| 963 | M1.6 | TITANIUM | 5.0 | 1 | SLOT COUNTERSINK | Provide pressure on button |
| 913 | M2 | TITANIUM | 3.0 | 2 | ALLEN GRUB SCREW | Wire clamping cooling plate |
| 913 | M2 | TITANIUM | 3.0 | 3 | ALLEN GRUB SCREW | Wire clamping cooling plate |
| 84 | M1.6 | TITANIUM | 2.0 | 1 | SLOT FASTENER | Wire clamping rotation stage 8 |

| | |
|---|---|
| FILE NAME SCREW_LIST.DWG | SHEET SHEET_17 / SCALE N/A |
| MATERIAL VARIOUS | LIST OF SCREWS |
| DRAWN 24/02/2016 | DRAWN BY EIRIK KJEKEN & SIMON COOIL |
| UNITS MM | |
| APPR. | |
| ISSUED | |
| REV REVISION_0 | NTNU - NT - IFY |
| MASTERS PROJECT | |

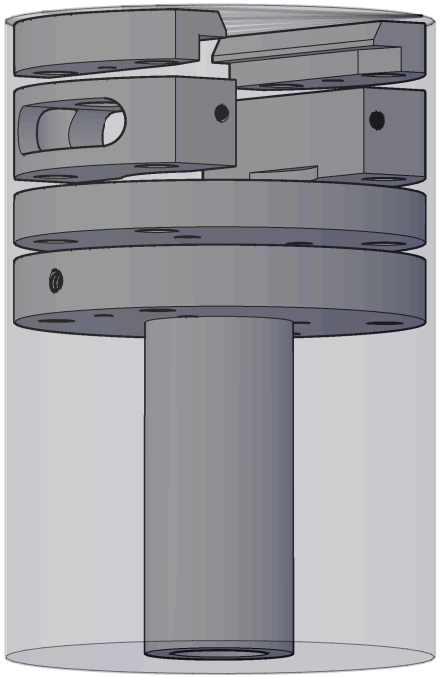

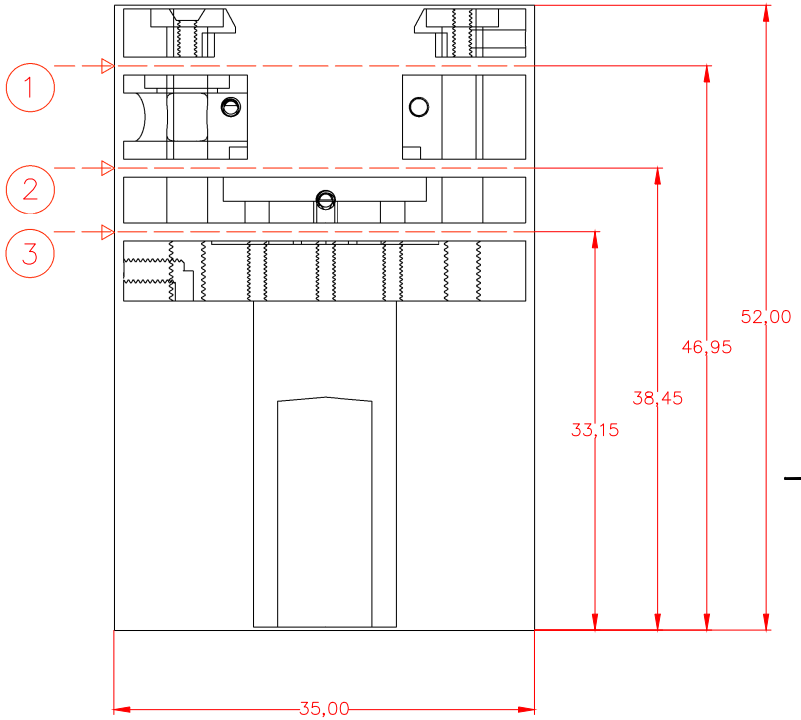


| | | | |
|---|---|---|---|
| FILE NAME | AZIMUTH STAGE CUT DIAGRAM 1 | SHEET | SHEET_18 |
| | | SCALE | 3:1 |
| MATERIAL | OXYGEN-FREE COPPER | | CUT DIAGRAM 1 |
| DRAWN | 17/02/2016 | | DRAWN BY<br>EIRIK KJEKEN & SIMON COOIL |
| UNITS | MM | | |
| APPR. | | | |
| ISSUED | | | |
| REV | REVISION_1 CHECKED BY JUSTIN WELLS | | NTNU - NT - IFY |
| CONTRACT NO | MASTERS PROJECT | | |

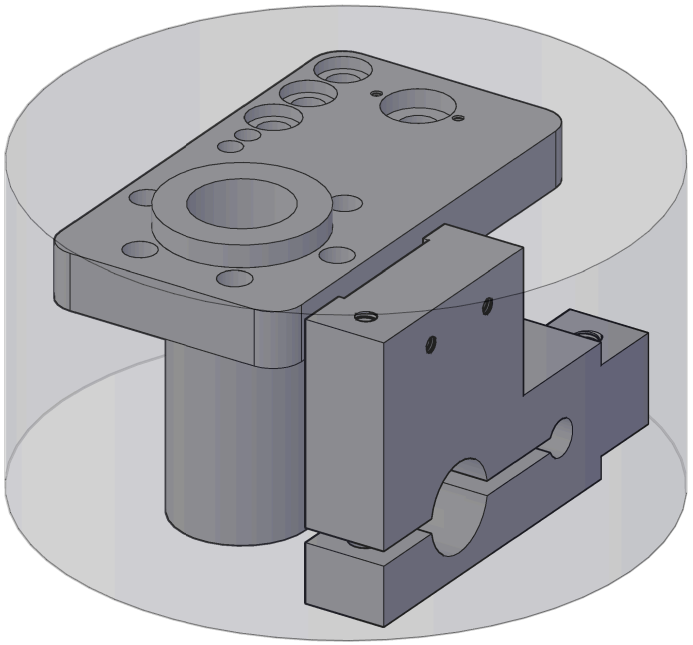

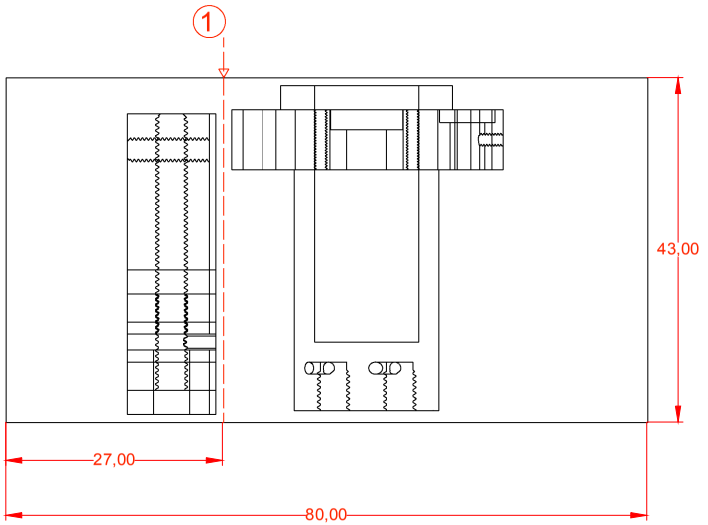


| | | |
|---|---|---|
| FILE NAME AZIMUTH STAGE CUT DIAGRAM 2 | SHEET SHEET_19 | SCALE 2:1 |
| MATERIAL OXYGEN-FREE COPPER | CUT DIAGRAM 2 | |
| DRAWN 17/02/2016 | DRAWN BY EIRIK KJEKEN & SIMON COOIL | |
| UNITS MM | | |
| APPR. | | |
| ISSUED | | |
| REV REVISION_1 CHECKED BY JUSTIN WELLS | NTNU - NT - IFY | |
| CONTRACT NO MASTERS PROJECT | | |

# II Additional Technical Drawings

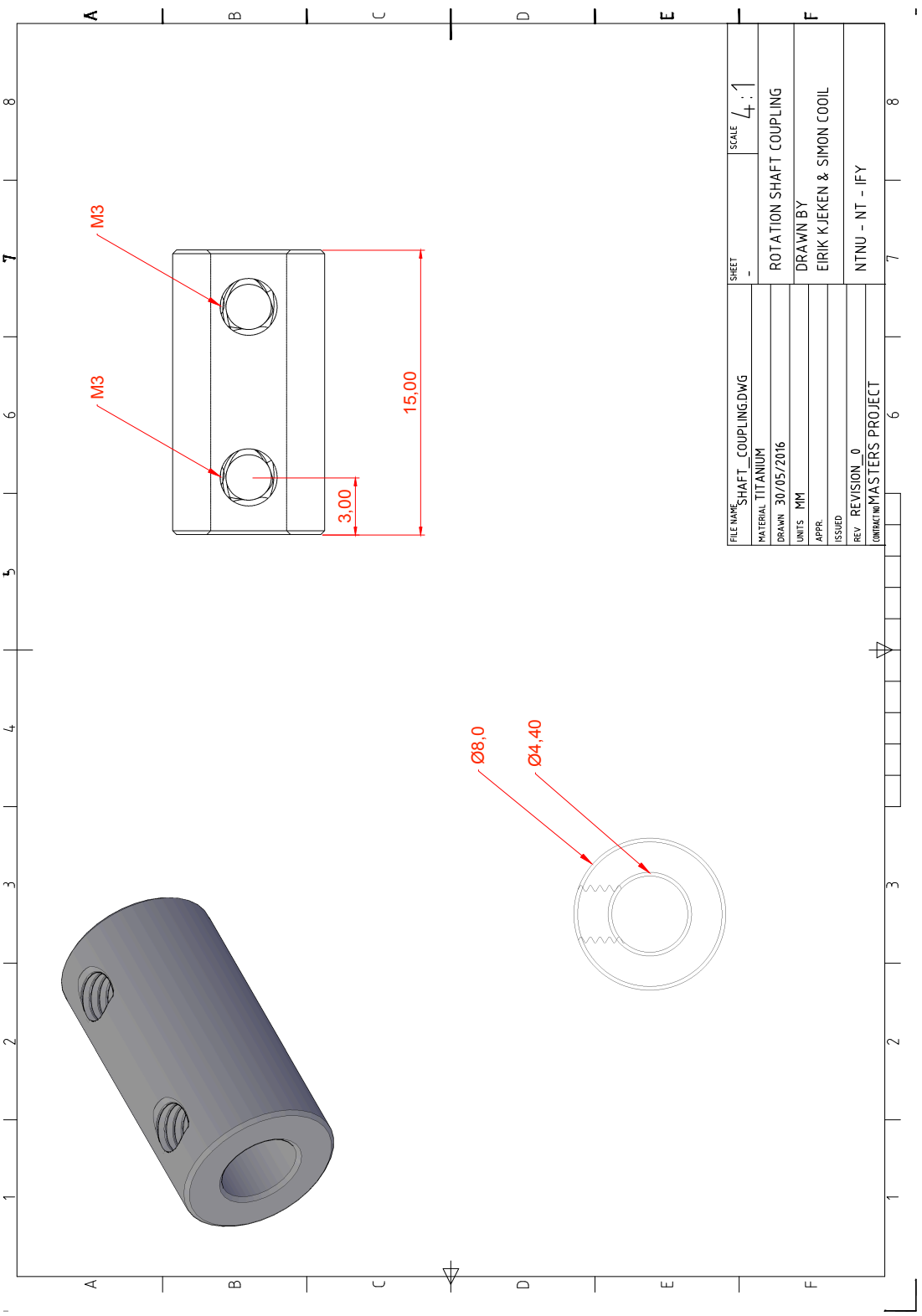

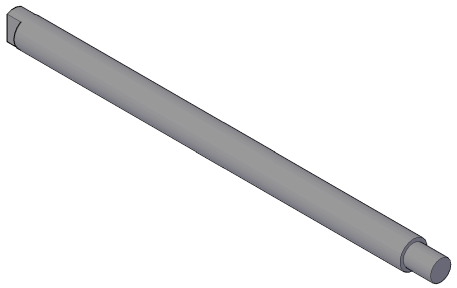

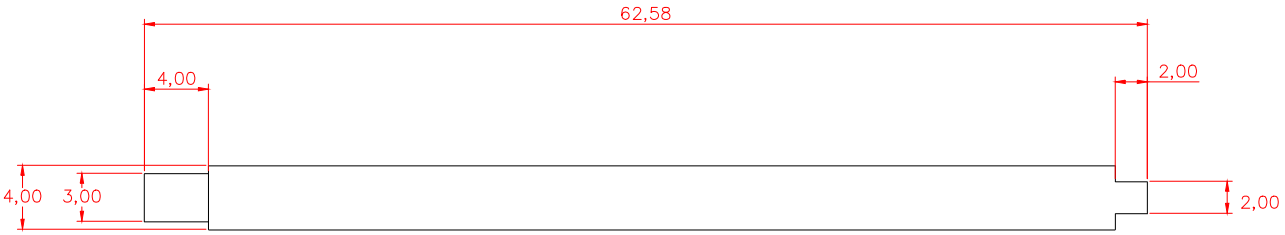


+ 454mm long ø3mm shaft

| | | |
|---|---|---|
| FILE NAME SHAFTS.DWG | SHEET - | SCALE 4:1 |
| MATERIAL STAINLESS STEEL | AZIMUTH ROTATION SHAFTS | |
| DRAWN 26/05/2016 | DRAWN BY EIRIK KJEKEN & SIMON COOIL | |
| UNITS MM | | |
| APPR. | | |
| ISSUED | | |
| REV REVISION_1 CHECKED BY JUSTIN WELLS | NTNU - NT - IFY | |
| CONTRACT NO MASTERS PROJECT | | |

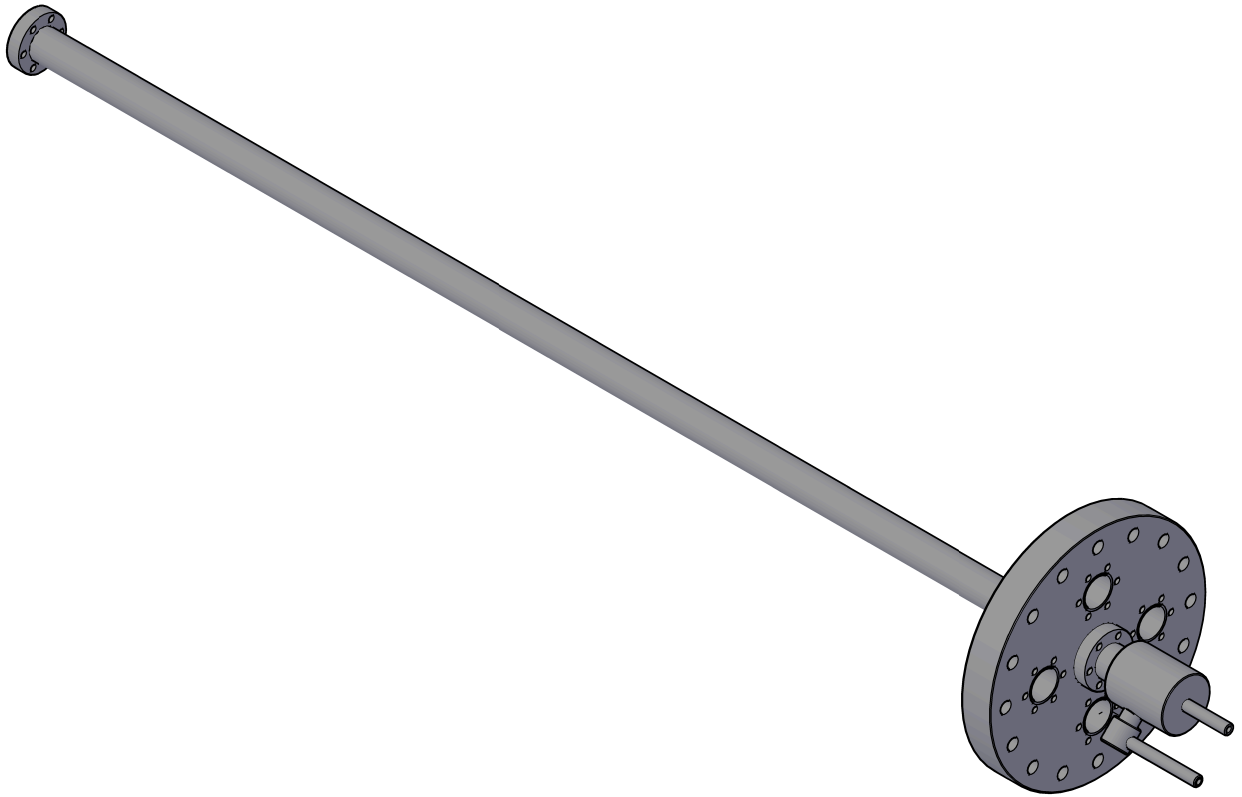

| | | | |
|---|---|---|---|
| FILE NAME CRYOSTAT V2 | SHEET SHEET_1 | SCALE 1:2 | |
| MATERIAL 304 STAINLESS STEEL | AZIMUTH LN2 CRYOSTAT V2 | | |
| DRAWN 21/02/2016 | | | |
| UNITS MM | DRAWN BY<br>EIRIK KJEKEN & SIMON COOIL | | |
| APPR. | | | |
| ISSUED | | | |
| REV REVISION_0 | NTNU - NT - IFY | | |
| CONTRACT NO MASTERS PROJECT | | | |

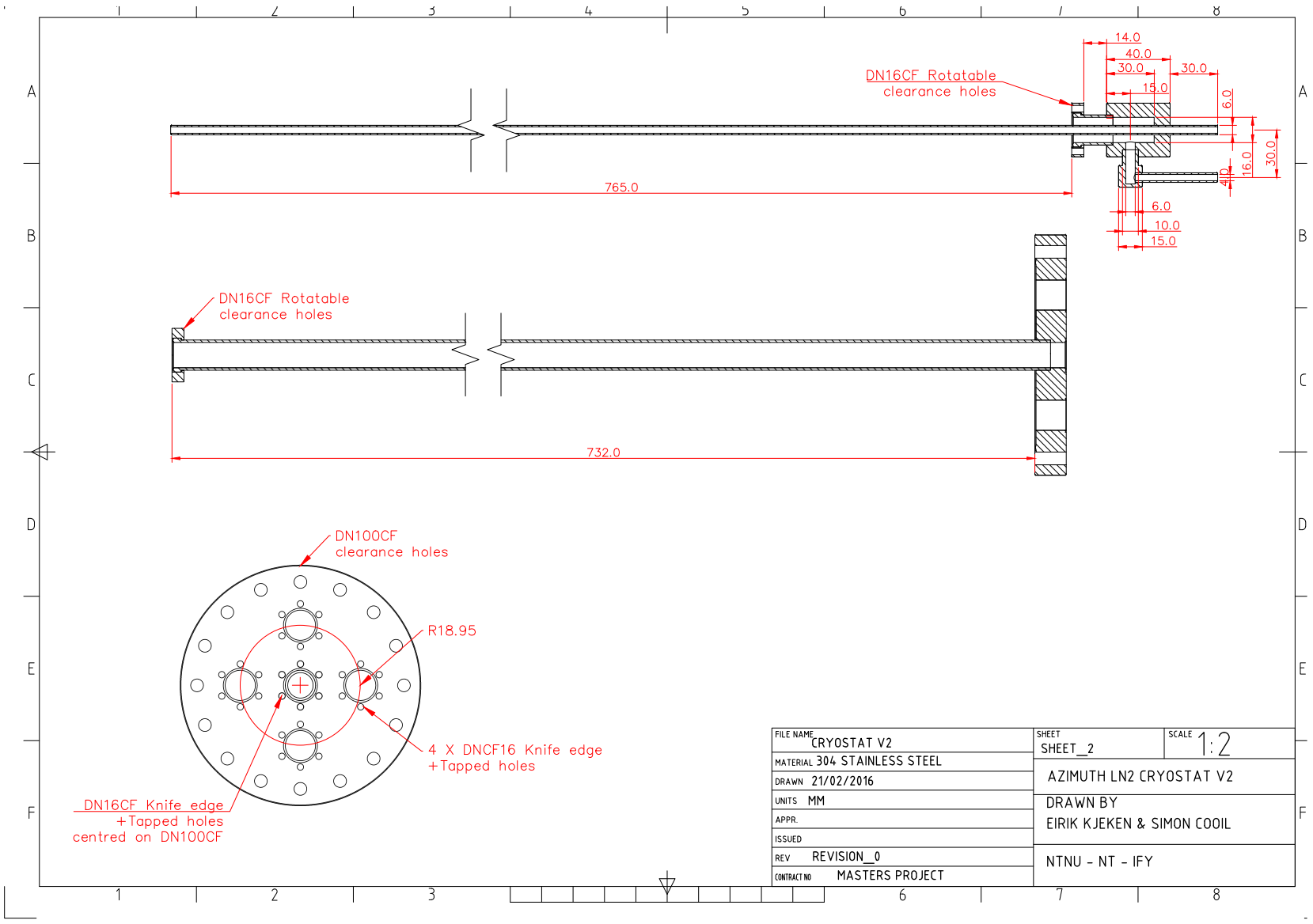


| | | |
|---|---|---|
| FILE NAME CRYOSTAT V2 | SHEET SHEET_2 | SCALE 1:2 |
| MATERIAL 304 STAINLESS STEEL | AZIMUTH LN2 CRYOSTAT V2 | |
| DRAWN 21/02/2016 | DRAWN BY<br>EIRIK KJEKEN & SIMON COOIL | |
| UNITS MM | | |
| APPR. | | |
| ISSUED | | |
| REV REVISION_0 | NTNU - NT - IFY | |
| CONTRACT NO MASTERS PROJECT | | |